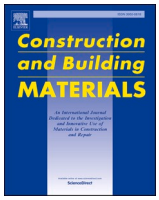
Construction and Building Materials 368 (2023) 130355



Contents lists available at ScienceDirect

Construction and Building Materials

journal homepage: www.elsevier.com/locate/conbuildmat





Studies on sol-gel bonded inorganic based plates having expanded lightweight inclusions for improving energy efficiency

Emre Yavuz [a,*], Niyazi Ugur Kockal [a], Ramazan Erdem [b]

[a] Akdeniz University, Department of Civil Engineering-Construction Materials, Antalya 07058, Türkiye
[b] Akdeniz University, Serik GSS Vocational School of Higher Education, Department of Textile Technologies, Antalya 07500, Türkiye

ARTICLE INFO

Keywords:
Expanded glass
Expanded vermiculite
Expanded perlite
Plate
Sol-gel
Thermal conductivity
and Fire resistance

ABSTRACT

Thermal insulation materials are a great solution to minimize energy consumption for construction applications. Especially, expanded inorganic lightweights are excellent candidates in terms of their low thermal conductivity and high fire resistance properties. Sol-gel type inorganic based binders are also useful chemical substances to combine lightweight particles. In current study, inorganic-based plates were developed by using expanded glass, expanded vermiculite, and expanded perlite particles with a novel tetraethoxysilan (TEOS)/methyltrimethoxysilane (MTMS) sol-gel binder. The chemical, physical, mechanical and thermal properties of the plates were examined comparatively to reveal the effect of expanded lightweight particle types in the plates. According to the experimental results, the compressive strength of the developed plates was between 7.04 ± 0.44 MPa and 3.15 ± 0.17 MPa whilst the direct tensile strength ranged from 0.486 ± 0.04 MPa and 0.079 ± 0.04 MPa, respectively. Furthermore, the long term water absorbency values of the plates on the 28th day varied between 9.96 ± 0.04 v% and 49.8 ± 0.8 v%. On the other hand, while the thermal conductivity coefficient of the plates at 25 °C ranged from 0.125 to 0.254 W/m.K, infrared reflectance properties were determined between 83.2 ± 0.5 % and 64.1 1.8 %. Besides, all inorganic-based plates exhibited high fire resistance performance (withstand temperatures of up to ~900 °C for 30 min). The results demonstrated that utilizing expanded inorganic lightweight particles with TEOS/MTMS sol-gel binder could be a promising combination to construct energy saving insulating plates to overcome poor fire resistance properties of conventional organic materials.

1. Introduction

The urban population is forcing cities to grow and become more complex than they were previously, which is escalating demand for housing, transportation, energy systems, and other infrastructure facilities. The rapid increase in population and technological advancements have resulted in serious resource depletion, which has triggered the energy shortages, negative impacts of climate change, and rising trend in greenhouse gas emissions. According to the IPCC's Fifth Assessment Report, if the necessary measures are not taken to lessen the quantity of carbon dioxide and other greenhouse gases in the atmosphere, the average earth surface temperature is predicted to rise by a range of 2.6 °C to 4.8 °C within the next 100 years, in correlation with the period from 1986 to 2005 [1]. On the other hand, authorities have emphasized the concerns about the current trends in energy consumption, and therefore, energy savings appears to be the most important aspect of energy efficiency. Especially, the construction sector attracts high attention of many researchers globally in terms of consuming huge amount of energy for heating and cooling of the buildings. The energy consumed for heating and cooling in buildings in the USA corresponds to 51 % of the total energy used in the buildings [2]. In Europe, this value is calculated as 40 % [3]. Furthermore, according to a study conducted in Australia (COAG National Strategy on Energy Efficiency), HVAC (heating, ventilation, and air conditioning) rates were reported as 49 % in office base buildings, 47 % in hospitals, and 50 % in universities [4]. Moreover, in Canada, the residential building consumed 17.1 % of total energy used in 2015 [5]. On the other hand, the global greenhouse gas emission rate created by the energy used to heat or cool buildings is calculated as 24 % of the total emission [6]. Consequently, thermal insulation materials have to be developed in order to minimize the energy consumption in buildings.

Commercial thermal insulation materials can mainly be examined in two classes as organic and inorganic. Organic materials such as polyurethane, XPS (extruded polystyrene), EPS (expanded polystyrene), etc.

* Corresponding author.
E-mail address: emreyavuz08@gmail.com (E. Yavuz).

https://doi.org/10.1016/j.conbuildmat.2023.130355
Received 18 September 2022; Received in revised form 24 December 2022; Accepted 8 January 2023
Available online 24 January 2023
0950-0618/© 2023 Elsevier Ltd. All rights reserved.

have low thermal conductivity values, however they show low resistance to fire [7]. Additionally, depending on the chemical composition of their structures, these organic materials decompose during a fire, producing hazardous gases like carbon monoxide (CO), hydrogen cyanide (HCN), hydrogen chloride (HCl), hydrogen bromide (HBr), and nitrogen dioxide (NO_2) [8]. When toxic fumes are released into the environment, they pose serious health risks when they are inhaled. As a result, when choosing a building material, it is crucial to take into account both the ignition temperature and smoke production. In contrast, inorganic lightweight expanded materials including expanded perlite, expanded vermiculite, and expanded glass, etc. possess low thermal conductivity, good durability, low cost, and high temperature resistance [9,10].

Expanded lightweight materials are generally yielded under the high temperature heat. Due to the aforementioned heat treatments, the volumes and porosity of the materials increase, thus their density decreases and thermal insulation properties are improved [11,12]. As a lightweight material, expanded perlite, which is an amorphous volcanic glass, is mostly composed of silica (SiO_2 70–76 %) and a trace quantity of other oxides (Al_2O_3, K_2O, Na_2O, Fe_2O_3) [13]. Because of the vast network of air bubbles that are formed during expansion, perlite flakes have a very low density. It is a very light substance with a very low loose bulk density. It has exceptional thermal, acoustic, and fire resistance, moreover, it is chemically resistant, and its properties are time-invariant. Consequently, expanded perlite has advantageous features due to its distinct microstructure, and have been used in many industrial applications such as heat-insulation products, agricultural components, and acoustic fillings [14,15]. Another attractive lightweight material is expanded vermiculite. As a raw material, vermiculite is a naturally occurring multilayered mica-like mineral with a 2:1 layer structure. It is mostly composed of SiO_2 (37–42 %), MgO (11–23 %), Al_2O_3 (10–13 wt %), Fe_2O_3 (5–17 wt%), and H_2O (8–18 %), though it can be obtained in many forms and structures depending on the geological conditions during its formation phase. A common formula for an idealized vermiculite is $(Mg, Fe^{2+}, Al)_3(Si,Al)_4O_{10}(OH)_2{\cdot}4H_2O$ [16–19]. Numerous benefits of vermiculite include its high abundance, environmentally benign nature, chemical inertness, flame retardancy, strong thermal stability, and prolonged operating life [20]. Other well-known lightweight material is expanded glass, also called hollow glass microspeheres, which has a small cellular structure and rigid porous inorganic beads containing air, produced by using recycled waste bottles and flat glass, is mostly constitute of amorphous silica (SiO_2, 71–73 %) and low amounts of other oxides (Al_2O_3, K_2O, Na_2O, CaO, MgO, Fe_2O_3 etc.) [21]. Due to their low thermal conductivity, high thermal stability, and light weight, expanded glasses are particularly desirable materials for widely used in many fields such as aerospace, construction, coating, etc. [22–24].

It has been reported in previous literature studies that various organic matrixes used to consolidate lightweight materials into plate form. On the other hand, researchers also used expanded lightweight materials as fillers to improve the properties of organic matrixes such as polypropylene [25–27], epoxy [28–30], polyurethane [31,32], phenolic resin [33,34], etc. Although these composites outlined above offer high mechanical properties, low density and thermal conductivity, they perform insufficient fire and high temperature resistance. To enhance the performance of the composites against fire and high temperature, inorganic based matrixes with lightweight expanded materials would be promising options.

In the group of inorganic based matrixes, there are generally cement-based ones, geopolymers, and sol-gel derived binders. Cement-based inorganic binders included materials are essential for the building industry due to their sufficient mechanical and thermal properties [35,36]. Many researches have been conducted regarding obtaining cement based inorganic binders. For instance; in an experiment conducted by Bumanis et. al. [37], they developed expanded perlite-based lightweight concrete using cement as a binder. The materials' thermal conductivity coefficient was determined to be 0.14 W/m.K and on the 28th day compressive strength was found to be 4 MPa. Koksal et al. produced cement based mortars using vermiculite and silica fume [38]. The thermal conductivity of the samples was determined to be 0.257 W/m K, and their compressive strength ranged from 3.9 MPa to 16.4 MPa. In concrete technology, cement is utilized as a binder, which has a significant impact on material quality. However, cement production emits a considerable amount of CO_2 (up to 8 % of total global CO_2 emissions) and consumes a huge amount of energy [39,40].

Among well-known inorganic binders, geopolymers are more environmentally friendly than cement binder which was firstly described by Davidovits in 1976 [41]. Some of these geopolymers can be categorised as substantial lightweight materials that are applicable to be utilized in construction technologies. Due to their high mechanical and thermal resistance properties they have been widely explored by the researchers [40,42,43]. In a study conducted by Vaou and Panias [44], expanded perlite was used to create porous foamy geopolymer thermal insulation materials in the presence of sodium hydroxide (NaOH) and hydrogen peroxide (H_2O_2). It has been determined that these highly porous materials with high fire resistance and low thermal conductivity coefficient (0.03 W/m.K) exhibited low mechanical properties (compressive strength 0.78 MPa). Medri et al. reported that they developed lightweight composite panels using expanded vermiculite with geopolymer binder. The study revealed that these panels had a thermal conductivity of approximately 0.2 W/m.K and a compressive strength of ~2 MPa. Furthermore, it was found that all samples exhibited heat resistance up to 800 °C [45]. Le et al. procured geopolymer foams using metakaolin, potassium hydroxide, chopped basalt fibers, silica sand, and silica fume. The thermal conductivity of the materials was 0.25 W/mK, the flexural and compressive strengths were 3.2 MPa and 5.4 MPa, respectively, and the materials were found to be highly fire resistant [46]. In literature, it has been stated that geopolymers have some drawbacks such as their complex manufacturing process and lack of stability [47].

In the sol-gel method, hydrolysis and polycondensation processes are used to transform a liquid "sol" phase into a solid "gel" phase. Therefore this technique offers advantages for the development of inorganic based binder materials, as it enables the use of wide range precursors. Furthermore, this method allows to operate the curing temperature, gives the materials sufficient mechanical strength, provides thermal and humidity resistance [48–50]. Besides, low-viscosity sol-gel binders wet the particles efficiently and form a thin film layer around them, thus causing a more intense bonding at the points where the particles come into contact with each other. A few studies have been done regarding developing expanded lightweight fillers with sol-gel inorganic based binder. Wang et al. produced thermal insulation plates based on expanded glass using aluminum-chrome-phosphate and tetraethyl orthosilicate as binders. The mechanical and thermal properties of the materials prepared at different sintering temperatures (250 °C to 650 °C) were investigated. The plates that were sintered at 450 °C were found to have a thermal conductivity of 0.062 W/m.K and the compressive strength was measured as 9 MPa [51].

The aim of the present research is to prepare and compare TEOS/MTMS sol-gel bonded inorganic based plates having expanded glass, expanded vermiculite, and expanded perlite as lightweight inclusions. The chemical, physical, mechanical and thermal properties of the developed plates were investigated.

2. Materials and methods

2.1. Materials

Tetraethoxysilane (TEOS) (Aldrich, 98 %) and methyltrimethoxysilane (MTMS) (ABCR, 97 %) were used as sol-gel binder precursors. Formic acid (Merck, 98–100 %) was used as catalyzer in the yielding process of binder. Within the current study, three different expanded lightweight particles were used as raw materials. Expanded glass (EG)

Table 1
Granulometric composition of the expanded lightweight particles.

Raw materials	Percentage passing						
	Sieve size (mm)						
	4.75	2.36	1.18	0.6	0.3	0.15	0.075
Expanded glass	100	100	100	100	99.65 ± 0.6	22.41 ± 0.6	0.41 ± 0.1
Expanded vermiculite	100	100	96.6 ± 0.1	78.57 ± 4.9	35.32 ± 4.3	4.17 ± 0.5	0.63 ± 0.03
Expanded perlite	100	99.6 ± 0.3	96.69 ± 0.3	66.32 ± 0.3	38.12 ± 0.3	15.09 ± 0.6	3.2 ± 0.1

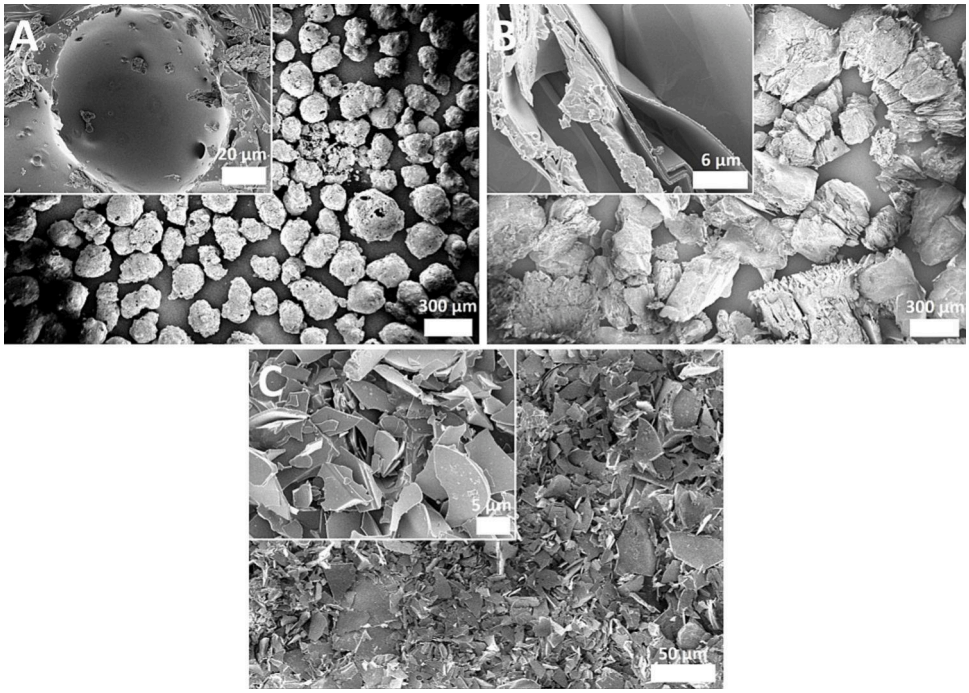


Fig. 1. SEM images of expanded lightweight particles (A) expanded glass, (B) expanded vermiculite, and (C) expanded perlite.

Table 2
Chemical compositions of expanded lightweight particles (wt%).

Raw material	SiO_2	Al_2O_3	CaO	Fe_2O_3	K_2O	TiO_2	SO_3	CI	MgO	Na_2O	P_2O_5	Other
Expanded glass	69.13	7.1	6.77	0.27	0.29	0.06	0.18	0.03	2.43	13.7	–	0.04
Expanded vermiculite	46.8	13.2	4.61	5.09	0.14	0.41	0.06	0.01	26.9	0.95	0.60	1.23
Expanded perlite	74.9	14.4	0.85	0.71	4.38	0.15	0.02	0.06	0.15	3.78	–	0.10

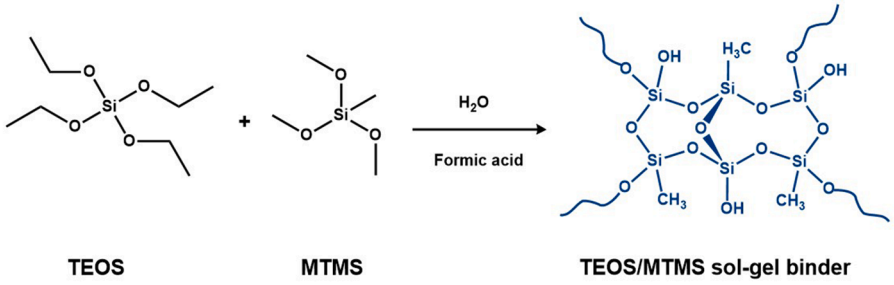


Fig. 2. Synthesis reaction mechanism of TEOS/MTMS sol–gel binder.

(400 kg/m^3) was purchased from Stikloporas (Lithuania). Expanded vermiculite (EV) (V0, 95–110 kg/m^3) was obtained from Agrekal (Türkiye). Expanded perlite (EP) (Perlisiol P05, 40–50 kg/m^3) was supplied by Genper (Türkiye). Particle size distributions of EG, EV, and EP are presented in Table 1. Also, SEM micrographs of the expanded lightweight particles are shown in Fig. 1. In the images, the EG particles were almost spherical in form, on the other hand, EV particles were longish rod-like in shape whereas the features of the EP particles were observed as debonded flakes. Furthermore, surface areas and average pore diameters of the expanded lightweight particles have been

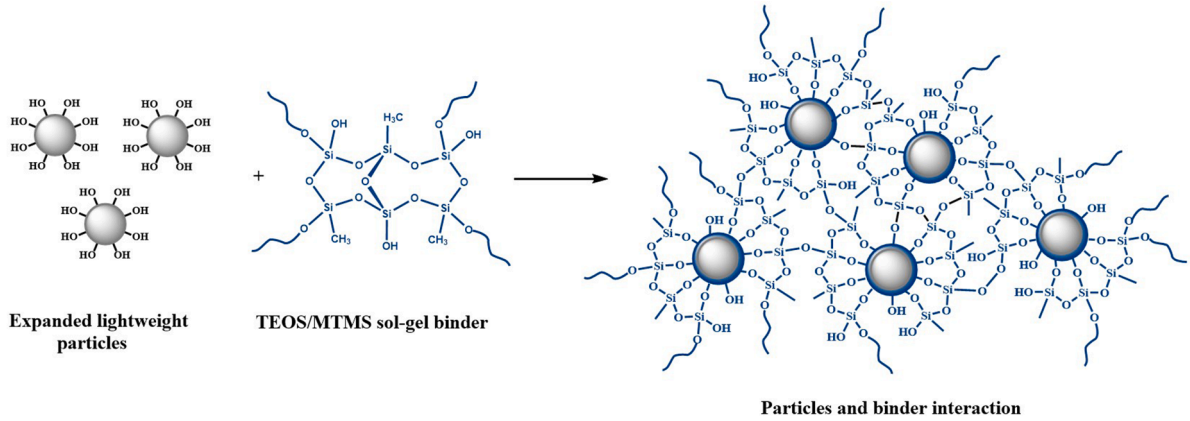


Fig. 3. Simplified illustration of expanded lightweight particles and TEOS/MTMS sol–gel binder reaction mechanism.

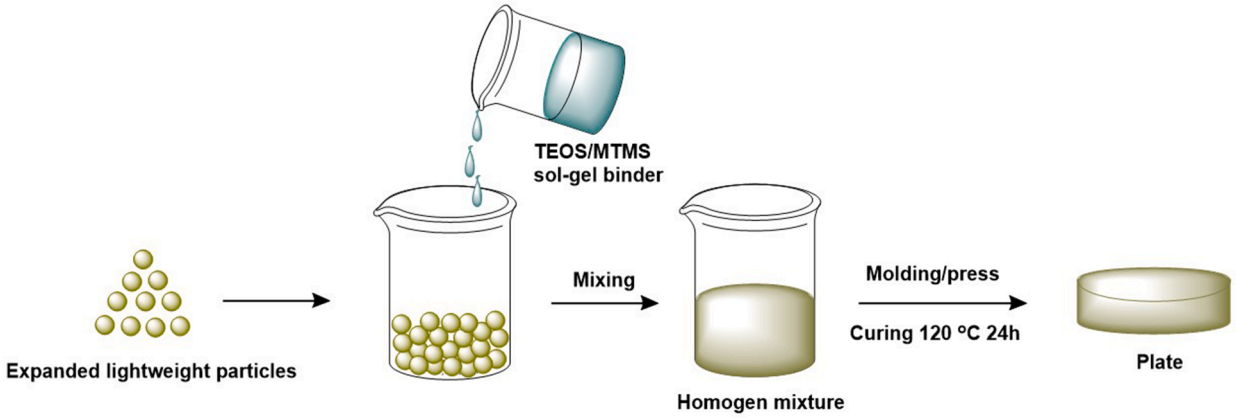


Fig. 4. Schematic diagram of the production steps of expanded lightweight base plates.

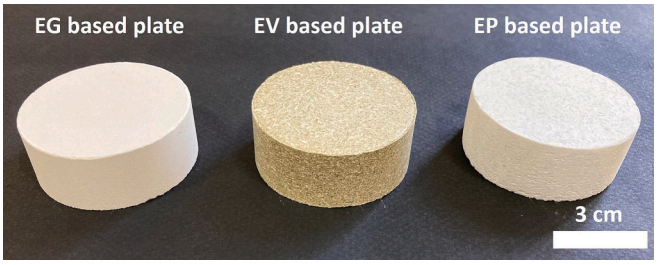


Fig. 5. Images of different inorganic based plates.

determined by BET analysis and they were found as 2.176 m^2/g and 6.28 nm for EG, 5.232 m^2/g and 10.65 nm for EV, and 6.745 m^2/g and 8.05 nm for EP. Results prove that all the expanded lightweight particles have mesoporous features. According to X-ray fluorescence spectrometer analysis, chemical composition of the EG, EV and EP is depicted in Table 2. As it is clearly seen that the main component of the expanded lightweight particles are SiO_2 which dominates at least 46.8 % of the total composition. On the other hand, major constituents have been determined as Na_2O in EG, and MgO (26.9 %) and Al_2O_3 (13.2 %) in EV, and Al_2O_3 (14.9 %) in EP, respectively.

2.2. Synthesis of TEOS/MTMS sol-gel binder

In this study, the binder matrix was prepared by sol-gel technique. Firstly, 81.201 g of TEOS, 156.395 g of MTMS ($n_{(MTMS])}/n_{(TEOS)}$:3) and 2.372 g of formic acid ($n_{(TEOS+MTMS])}/n_{(formic\ acid)}$:3), were stirred together. Then 89.496 g of deionized water (n_{alcoxy}/n_{water}:1) were added dropwise during stirring at 750 rpm, and this solution continued to be stirred for 2 h at room temperature in order to obtain the binder solution. Eventually, a series of hydrolysis and polycondensation reactions between TEOS and MTMS resulted in an inorganic based matrix with high binding property. The synthesis mechanism of the binder is illustrated in Fig. 2.

2.3. Preparation of inorganic based plates

40 g of expanded lightweight particles were mixed with 15 g of TEOS/MTMS sol-gel binder and blended until homogeneous mixtures were obtained. Simplified reaction mechanism of binder and expanded lightweight particles is illustrated in Fig. 3. The obtained mixtures were placed in a cylinder mold (Ø 50 mm) and compressed (20 bar) for 1 min. Then the pressed samples were removed from the mold and cured at 120 °C for 24 h. The schematic diagram of the production steps and the images of the prepared plates are given in Fig. 4 and Fig. 5, respectively.

2.4. X-ray fluorescence spectrometer analysis

The chemical composition of expanded lightweight particles were determined by X-ray fluorescence spectrofotometer (Rigaku NEX CG, XRF, experimental error <0.2 %). The pellets for the XRF analysis (Ø 40 mm) were prepared with 0.1 % (wt/wt) sample in boric acid at 20 MPa.

2.5. BET surface area

To analyze surface areas and pore sizes of expanded lightweight

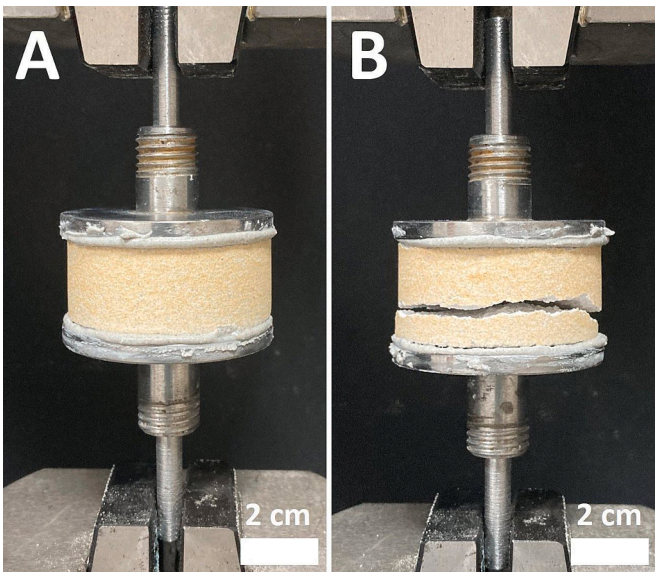


Fig. 6. Direct tensile strength test of the plates. (A) before the test and (B) after the test.

particles, Brunauer-Emmett-Teller (BET) measurements were carried out with a 3P Micro 300 gas adsorption instrument using nitrogen gas at 77.35 K by utilizing 3P Surface Area & Pore Size Analyzer Software.

2.6. X-ray diffraction analysis

X-ray diffraction (XRD) analysis was performed to determine the crystal and amorphous structures of expanded lightweight particles and the prepared plates by X-ray diffractometer (Shimadzu, XRD-6000). Cu-Kα X-ray radiation (1,544 Å) was utilized for the measurements in the range from 10° to 80° with scan speed 2 (deg/min). Patterns were correlated with the patterns indicated in The International Centre for Diffraction Data (ICDD) database.

2.7. Thermogravimetric analysis

In order to investigate the thermal durability characteristics of the expanded lightweight particles and the prepared plates, thermogravimetric analyses (TGA) were realized by Mettler Toledo TGA/DSC 3 + equipment at a heating rate of 10 °C/min. under nitrogen atmosphere between 25 and 1000 °C.

2.8. FT-IR analysis

The chemical structure of the expanded lightweight particles and the prepared plates were characterized by Fourier transform infrared (FT-IR) spectroscopy (Tensor 27) in transmission mode ranging from 400 to 4000 cm^{-1} at a resolution of 4 cm^{-1}. Transmittance spectra of powder samples were recorded by using KBr pellet technique. All pellets were prepared with 0.1 % (wt/wt) sample in KBr. In addition, transmittance spectra for liquid based samples were determined by using a horizontal attenuated total reflectance (HATR) device.

2.9. SEM-EDX analysis

The morphological features of the expanded lightweight particles and the prepared plates were explored by scanning electron microscopy (SEM; LEO 1530) and energy-dispersive X-ray spectroscopy (EDX, Aztec, Oxford Instruments). The samples were coated with a thin gold palladium layer (9 nm) using a sputter coater before the analysis.

2.10. Compressive strength

Compressive strengths of the prepared plates were determined by Universal testing machine (Utest, 100 kN), operating with a cross-head speed of 4 mm/min., according to modified version of BS EN 826 [52] test protocol. The compression tests were performed on cylindrical samples (Ø 50 mm) with a height of 20 mm. Each test was conducted in triplicate and the test results were averaged. Compressive strength of the plates were calculated by equation 1:

$$\sigma_c = \frac{F_m}{A_0} \quad (1)$$

where; σ_c represents compressive strength (MPa), F_m is the maximum force (N) and A_0 is the initial cross-sectional area of the specimen (mm^2).

2.11. Direct tensile strength

Tensile strengths of the prepared plates were explored by Universal testing machine (Utest, 100 kN), operating with a cross-head speed of 10 mm/min., according to modified version of BS EN 1607 [53] test protocol. In the analysis, both sides of the cylindrical samples (Ø 50 mm) with 20 mm height were adhered to 50 mm diameter cap screws with Epomortar FC510 two-component epoxy glue (Fig. 6). Each test was performed in triplicate and test results were averaged. Tensile strengths of the plates were calculated by equation 2:

$$\sigma_T = \frac{F_m}{A_0} \quad (2)$$

where; σ_T represents tensile strength (MPa), F_m is the maximum tensile force (N) and A_0 is the initial cross-sectional area of the test specimen (mm^2).

2.12. Apparent density

Apparent densities (ρ, g/cm^3) of the prepared plates were calculated according to BS EN 1602 [54]. Volume of the samples (Ø 50 mm) with 20 mm height was geometrically measured by means of three times for per side, utilizing a digital caliper (accuracy ± 0.01 mm). Each test was realized in triplicate, and test results were averaged.

2.13. Contact angle measurement

To determine the hydrophobic properties of the prepared plates, the contact angle values of the samples against water were determined using the Goniometer (Rame-hart/Model 100–00).

2.14. Surface roughness measurement

Mobile roughness measuring instrument (Mahr, MarSurf PS 10) was utilized to determine the average roughness (Ra, μm) of the plates according to stylus technique where the measurements have been taken from three different directions by 5 μm diamond stylus angled at 90° for each sample. Each test was realized in triplicate, and the test results were averaged.

2.15. Long-term water absorption

Long-term water absorption properties of the prepared plates were determined according to BS EN 12087 [55]. Briefly, the samples (Ø 50 mm) with 20 mm height were totally immersed in distilled water at 25 °C for 1, 7, 14, 21 and 28 days. At each predetermined time point, the samples were taken out from the water and dried for 10 ± 0.5 min., inclined at 45°, in ambient atmosphere. Then, all the samples were weighed and the differences were recorded. Long-term water absorption

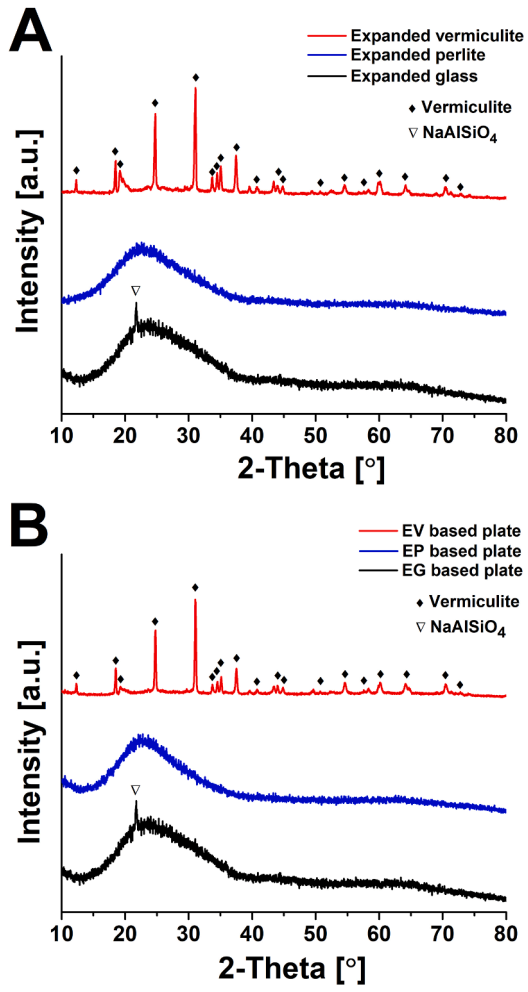


Fig. 7. XRD patterns of expanded lightweight particles and inorganic based plates. (A) EG, EV, and EP particles and (B) EG, EV and EP based plates.

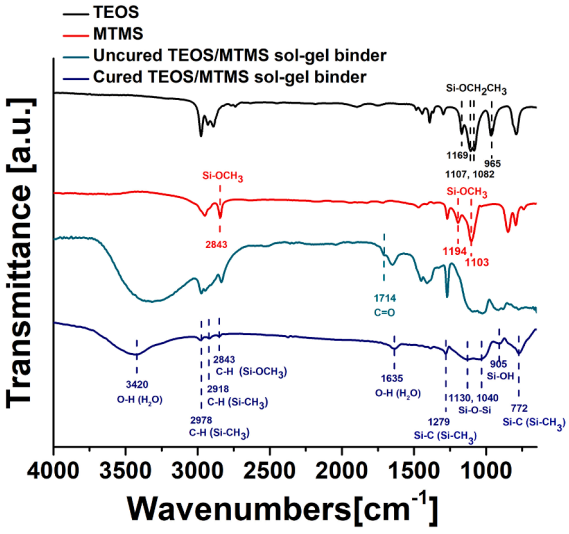


Fig. 8. FT-IR spectrum of TEOS, MTMS, and uncured and cured TEOS/MTMS sol–gel binders.

(W) of the plates were calculated by equation 3:

$$Wx = \frac{m_x - m_0}{V} X \frac{100}{\rho_w} \quad (3)$$

where; m_0 is the initial mass (g) of the plate, m_x is the mass of the plate after total immersion for X days, V is the initial volume (cm^3) of the plate, ρ_w is the density of water (g/cm^3) and W_x is long-term water absorption (v%).

2.16. Thermal conductivity analysis

Thermal conductivity coefficient (λ) analyses of the prepared plates (Ø 50 mm) were performed according to TS EN 12664 [56] standard by FOX50 test equipment between 0 °C and 90 °C.

2.17. Flame behavior of inorganic based plates

The flame behaviors of the prepared plates were evaluated by according to modified version of DIN 4102 [57] test protocol. Briefly, the flame (~900 °C) was applied at 90 °C into the central area of the sample surface (Ø 50 mm with 20 mm height) from a distance of 3 cm for 30 min. During the procedure, the effect of the flame on the samples and also the temperature change on the back surface of the plates were recorded by infrared thermometer (SKP, TKTL 30).

2.18. NIR-reflective properties of inorganic based plates

Spectral reflectance and band gaps (Eg) of the prepared plates were measured by UV–vis-NIR Spectrophotometer (Varian Cary 5G) using PTFE (Poly Tetra Fluoro Ethylene) as reference. NIR reflectance (R_{NIR}, %) which takes the solar spectrum (in between 700 and 2500 nm) into account was calculated according to ASTM E903 [58] (equation 4) in order to give a standard comparison between the reflectivity of different plates.

$$R_{NIR}(\%) = \frac{\int_{700}^{2500} RId\lambda}{\int_{700}^{2500} Id\lambda} x\,100 \quad (4)$$

where R_{NIR} is the percentage of reflectance, I is solar spectral irridance ($W.m^{-2}.nm^{-1}$) obtained from ASTM G173 (Air Mass 1.5) [59], and dλ is the wavelenght interval of integration. On the other hand, the band gaps of the plates have been calculated by Kubelka-Munk method [60,61]. Besides, the NIR reflective efficiency of the plates was performed in a self-designed set-up. The plates were exposed to radiation (0.58 $W.cm^{-2}$) under infrared lamp (250 W, Philips) where the distance between the samples and the lamp was set as 15 cm. The power of lamp was calibrated by Coherent 300 W laser Power/Energie meter, LabMax-Top. The alterations of the surface temperatures of the plates were recorded by an infrared camera (VarioCAM HD Thermography Infrared Camera).

3. Results and discussion

3.1. X-ray analysis

The mineralogical phases of expanded lightweight particles and the prepared plates are illustrated in Fig. 7. The observed broad hump between 10 and 35° in Fig. 7A demonstrates that both EG and EP consist of significant amount of SiO_2 amorphous phases [62–64]. XRD figure of EV also exhibits a spectrum belong to vermiculite which proves a crystalline structure and related characteristic diffraction peaks have been observed at 12.2°, 18.5°, 19.2°, 24.7°, 31°, 33.8°, 34.4°, 35.1°, 37.5°, 40.7°, 44°, 44.9°, 50.7°, 54.6°, 57.5°, 60°, 64.1°, 70.5°, and 72.8° (ICDD 00–060-0341). The recorded peak at 21.6° in the spectrum of EG was most probably associated with sodium aluminosilicate ($NaAlSiO_4$) in the

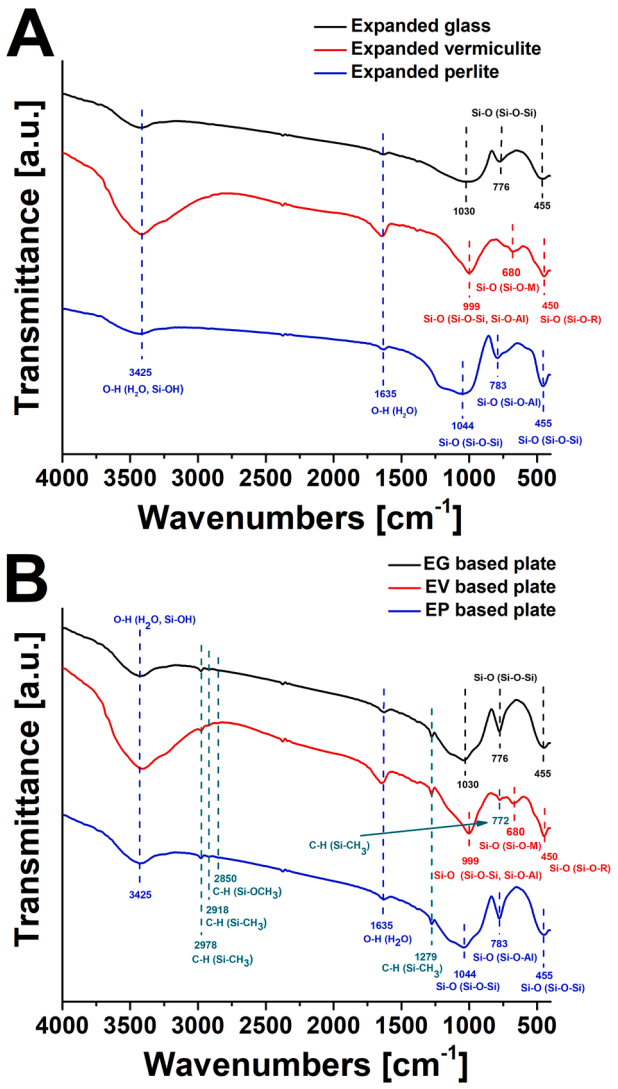


Fig. 9. FT-IR spectrum of expanded lightweight particles and inorganic based plates. (A) EG, EV, and EP particles and (B) EG, EV and EP based plates.

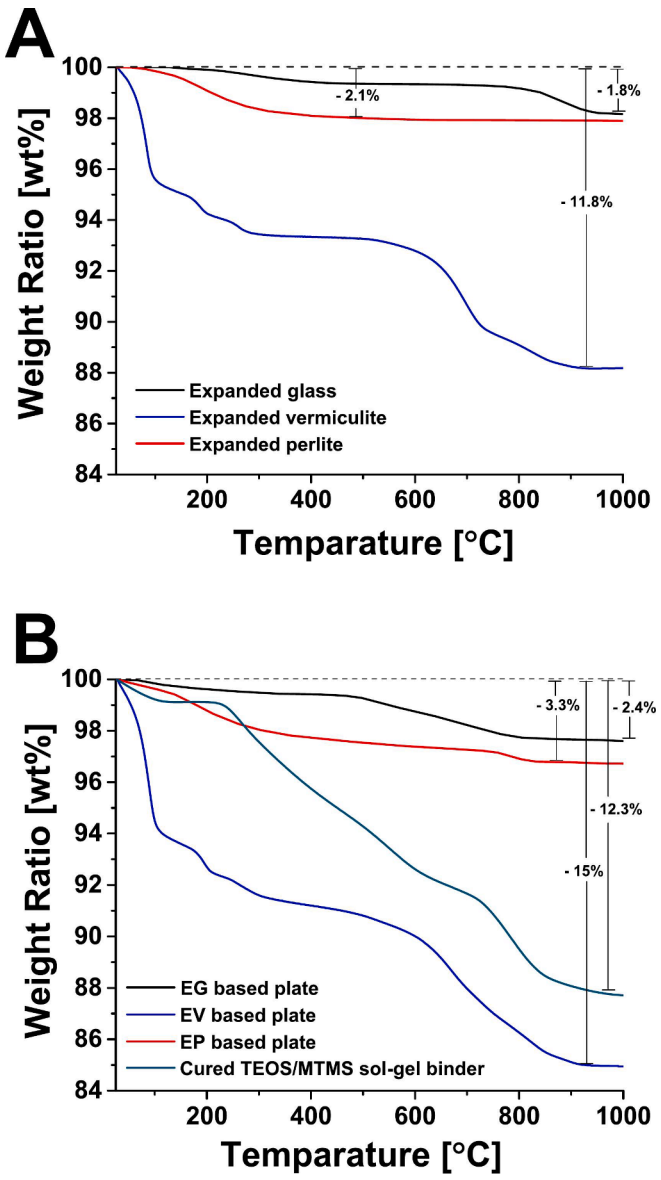


Fig 10. TGA curves of expanded lightweight particles, cured TEOS/MTMS sol–gel binder, and inorganic based plates. (A) EG, EV, and EP particles, (B) cured binder, EG, EV, and EP based plate.

structure [65]. Comparing XRD analyses in both Fig. 7A and B, it has been confirmed that the TEOS/MTMS sol-gel binder used in the system and the curing processes of the plates did not alter the original crystalline and amorphous structures of the expanded lightweight particles.

3.2. FT-IR analysis

Structures of synthesized TEOS/MTMS sol-gel binder and developed inorganic based plates were characterized by using FT-IR spectroscopic analysis. The FT-IR spectra of TEOS, MTMS, and uncured and cured TEOS/MTMS sol-gel binder are exhibited in Fig. 8. The sharp peak at 965 cm^{-1}, strong double peaks at 1082 and 1107 cm^{-1} and the peak at 1169 cm^{-1} are assigned with the Si-OCH_2CH_3 group of TEOS. Strong peaks at 1103 cm^{-1}, 1194 cm^{-1} and sharp peaks at 2843 cm^{-1} characterize the Si-OCH_3 group in MTMS. When the spectrum of the cured TEOS/MTMS sol-gel binder is examined, it is seen that the peaks of the alkoxy (Si-OCH_2CH3 and Si-OCH_3) groups disappear after the hydrolysis and condensation reactions between TEOS and MTMS. Parallel to this, peaks at 772 cm^{-1} and 1279 cm^{-1} belonging to the non-hydrolyze Si-CH_3 groups in the silica oxide network occurred, as well as two distinct large symmetrical and asymmetric stretching peaks at 1040 cm^{-1} and 1130 cm^{-1} proves that Si-O-Si groups have been formed [66–69]. Other important peaks of the structure are the asymmetric and symmetrical C—H stretching of the –CH_3 group at 2978 cm^{-1} and 2918 cm^{-1} [70,71]. The symmetrical C—H stretching of the Si-OCH_3 group observed at 2843 cm^{-1} indicates that the methoxy groups belonging to MTMS in the binder have not been completely hydrolyzed. In addition, the wide peak observed at 905 cm^{-1}, in the range of 950–810 cm^{-1}, refers to the presence of Si-OH groups that remained without condensation in the structure. The O—H stretching and H—O—H bending of the H-bond observed at 3420 cm^{-1} and 1635 cm^{-1} correspond to the absorbed water [71,72]. The carbonyl (C═O) group observed at 1714 cm^{-1} in the FT-IR spectrum of the uncured TEOS/MTMS sol-gel binder is associated with the formic acid used as a catalyst in the binder synthesis which has been disappeared after curing [73].

The FT-IR spectra of expanded lightweight particles and inorganic based plates are compared in Fig. 9. The bands appeared in the range between 3750 cm^{-1} and 2900 cm^{-1} are characteristic of O—H stretching vibrations, whilst the range of 1500–400 cm^{-1} is corresponded to the finger print region which is definitive structural characteristics of materials. For all materials, the strong and wide peak observed at 3415 cm^{-1} is belonged to stretching vibrations of hydrogen bonding of silanol

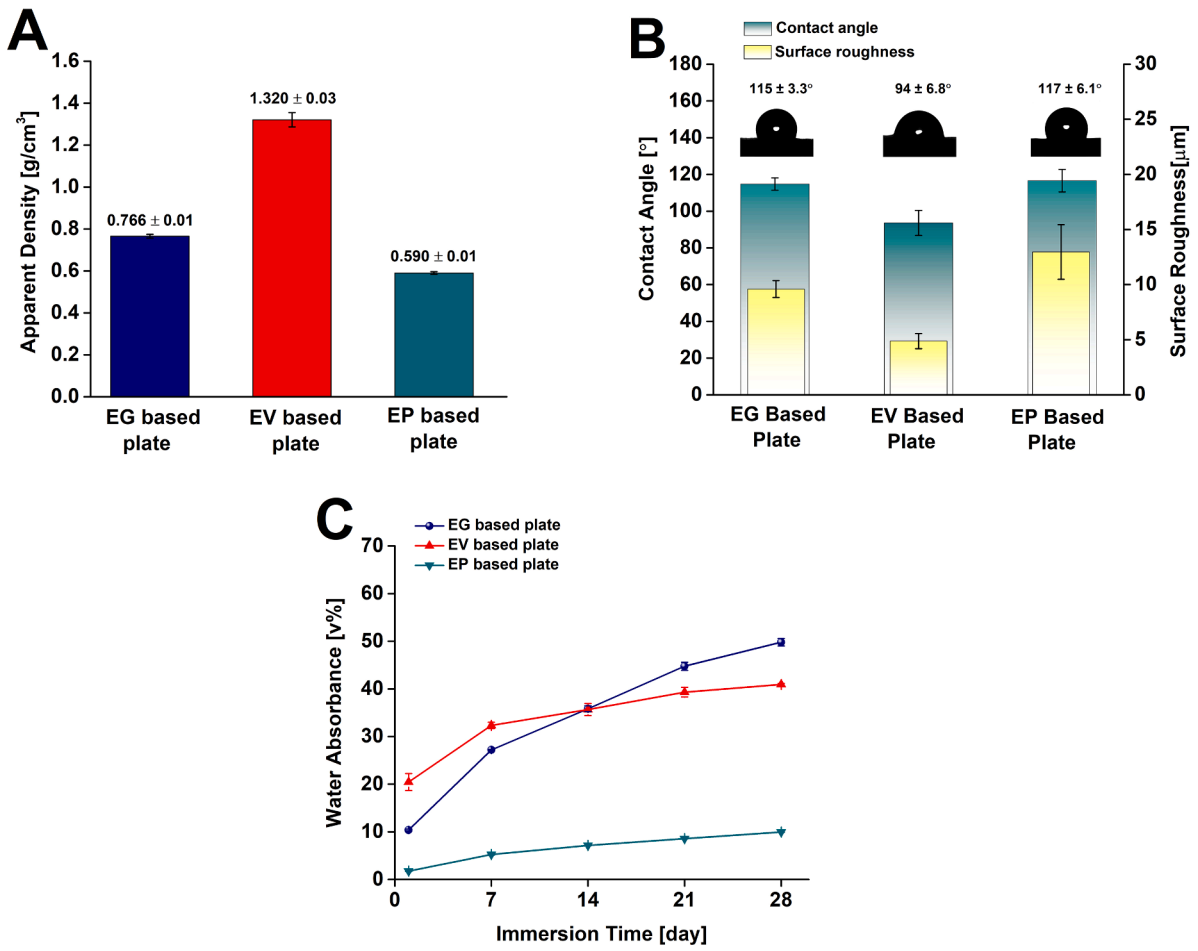


Fig. 11. EP, EV, and EP based plates properties. (A) Apparent density, (B) surface contact angle and rougness, and (C) long-term water absorption.

(Si-OH) groups and absorbed water on the particle surface. In addition, the peak at 1635 cm^{-1} characterizes the bending vibration of the water [66,74,75]. When the FT-IR spectrum in Fig. 9A is examined, five main absorption peaks of EG are observed. These indicate the presence of O—H, Si-OH and Si-O-Si groups in the structure. The strong peaks observed at 1030 cm^{-1}, 776 cm^{-1} and 455 cm^{-1} are associated with Si-O asymmetric stretching, bending and rocking vibration modes of Si-O-Si, respectively [76–78]. In the same figure, five characteristic absorption peaks of EV are detected. These prove the existence of O—H, Si-OH, Si-O-M (M: Al, Mg and Fe) and Si-O-R (R: Si, Al, Mg and Fe) groups in the structure. The most intense band at 999 cm^{-1} is assigned to Si-O stretching vibration of Si-O-Si and Si-O-Al [79–81]. The peaks appeared at 680 cm^{-1} and 450 cm^{-1} are corresponded to Si-O vibrations of Si-O-M [82,83] and Si-O-R, respectively [83–85]. Furthermore, FT-IR spectra illustrates the five main absorption peaks of EP that determine the presence of O—H, Si-OH, Si-O-Si and Si-O-Al groups in the structure. The peak observed at 1044 and 455 cm^{-1} belong to Si-O stretching and bending vibrations of Si-O-Si, subsequently. Besides, the recorded peak at 783 cm^{-1} indicates the Si-O stretching of Si-O-Al [62,74,86,87]. On the other hand, Fig. 9B depicts the FT-IR spectrum of EG, EV, and EP based plates where the characteristic peaks in finger print region are almost the same comparing with the spectra illustrated in Fig. 9A, however, there are some specific differences observed due to the binder addition into the plate composition. For instance; the asymmetric and symmetrical stretching, symmetric deformation vibrations and stretching vibration of the non-hydrolyzed Si-CH_3 group observed at 2978, 2918, 1279 and 772 cm^{-1}, respectively [88–90]. Also, the peak at 772 cm^{-1} could not be detected for EG and EP based plates because of the overlapping band of Si-O which cover the entire region. Moreover, the unhydrolyzed methoxy groups of MTMS, which is one of the compounds of the binder, has been detected as symmetrical C—H stretching peak at 2850 cm^{-1}.

3.3. TGA analysis

The weight loss of expanded lightweight particles are depicted in Fig. 10A. The total weight loss of EG, EV, and EP were recorded approximately as 1.8 %, 11.8 %, and 2.1 % between 25 and 1000 °C. In the case of EG, approximately ~1 % mass loss at 670–970 °C suggests that sodium carbonate (Na_2CO_3) decomposes to Na_2O and CO_2 [91–93]. The presence of Na_2CO_3 in the EG can be explained by the carbonation reaction occurring in two steps (see reactions 1 and 2) [94]. Briefly, Na_2O (13.7 %, Table 2) in the composition reacts with the absorbed H_2O and turns into sodium hydroxide (NaOH). Na_2CO_3 is then formed by the reaction of NaOH with atmospheric CO_2. It may be due to the amount of Na_2CO_3 out of the detection limit, the resulting Na_2CO_3 could not be detected by XRD analysis. Also, the remaining mass loss (0.8 %) belongs to the adsorbed water in the structure.

$$Na_2O + H_2O \rightarrow 2NaOH \quad (1)$$

$$2NaOH + CO_2 \rightarrow Na_2CO_3 + H_2O \quad (2)$$

According to the curves in Fig. 9A, EV exhibited three stages of thermal mass loss where the first two are related to dehydration and the third one is assigned to dihydroxylation [95–97]. The first stage occurred from 25 °C to 110 °C with a weight loss of 4.68 %, which is attributed to physically adsorbed water molecules on the surface. Second dehydration stage is corresponded to removal of interlayer water

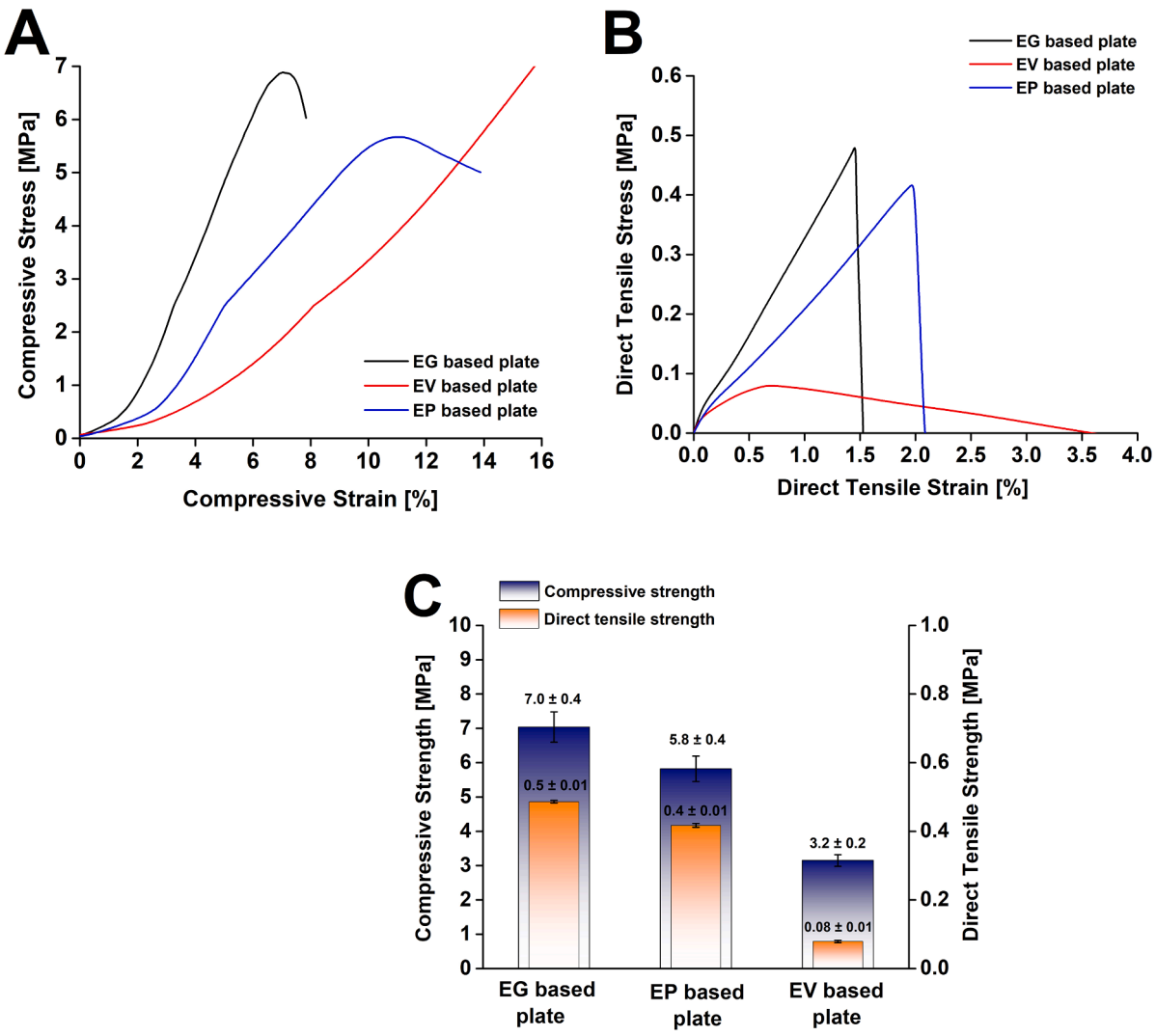


Fig 12. Mechanical properties of the inorganic based plates. (A) compressive stress–strain curves, (B) direct tensile stress–strain curves, and (C) comparision of comprassive and direct tensile strenghts.

between 110 °C and 300 °C with a weight loss of 1.89 %. At the third stage, the mass change of 5.26 % is relevant to removal of water in the crystal structure of vermiculite during dehydroxylation reaction which occurred between 500 and 920 °C. On the other hand, the decline in the mass of EP between 25 and 150 °C is linked to the loss of adsorbed water (0.5 %). The largest mass loss of 1.59 % occurs in the temperature range of 150–450 °C which is probably due to the release of inter-packeted water. The temperature range limits cannot be rigorously specified due to the perlite's complexity and the variety of interactions between water/–OH groups and the matrix, as illustrated in Fig. 10A [98].

The TGA results of prepared plates and cured TEOS/MTMS sol-gel binder are shown in Fig. 10B. The cured binder exhibits 0.9 % mass loss between 25 and 130 °C which was attributed mainly to the evaporation of adsorbed water in the gel. Between 200 and 1000 °C the weight loss (11.4 %) can be ascribed to the condensation reaction of remaining Si-OH and alkoxy (Si-OCH_2CH_3 and Si-OCH_3) groups, and pyrolysis of methyl groups [99–101]. The total mass loss of plates between 25 and 1000 °C was revealed to be higher compared to the raw materials where the losses of EG, EV, and EP based plates were recorded are 2.4 %, 15 %, and 3.3 %, respectively. The losses can be explained by two principal changes. Firstly, gradual mass loss until 300 °C was attributed to the evaporation of physical bonded water. Second, the mass loss between 350 and 1000 °C is mainly corresponded to pyrolysis of methyl groups and condensation reaction of residual Si-OH and alkoxy groups which occurs as a result of Si-O-Si chain reordering.

3.4. Physical properties of inorganic based plates

In general, apparent density is a crucial factor that influences the mechanical and thermal properties of materials [102–105]. The apparent densities of EG, EV, and EP based plates are depicted as 0.766 ± 0.01 g/cm^3, 1.320 ± 0.03 g/cm^3, 0.590 ± 0.01 g/cm^3, respectively in Fig. 11A. Various findings have been found when the literature on this subject is reviewed. For instance; EG-containing alkali-activated composites were prepared by Tatlsu et al. [106], and the apparent density values of the samples ranged from 0.21 to 0.86 g/cm^3. Medri et. al. [45] obtained EV based alkali-activated plates and the apparent densities of the structures were determined to be between 0.7 and 0.9 g/cm^3. Vaou et. al. [44] procured perlite included alkaline activated foam and the density of the foam ranged from 0.335 to 0.665 g/cm^3.

According to contact angle phenomenon, surfaces are hydrophilic if the angle is below 90°; however, the surfaces become hydrophobic as the angle exceeds 90°. Another relevant matter is that the rising surface energy causes a downward tendency in contact angle [107,108]. Contact angle test results and shapes of the water drops on the surfaces of the inorganic based plates are exhibited in Fig. 11B. Findings revealed that the greatest value (117 ± 6.1°) has been obtained for EP based plates whereas the lowest angle degree (94 ± 6.8°) has been yielded for EV

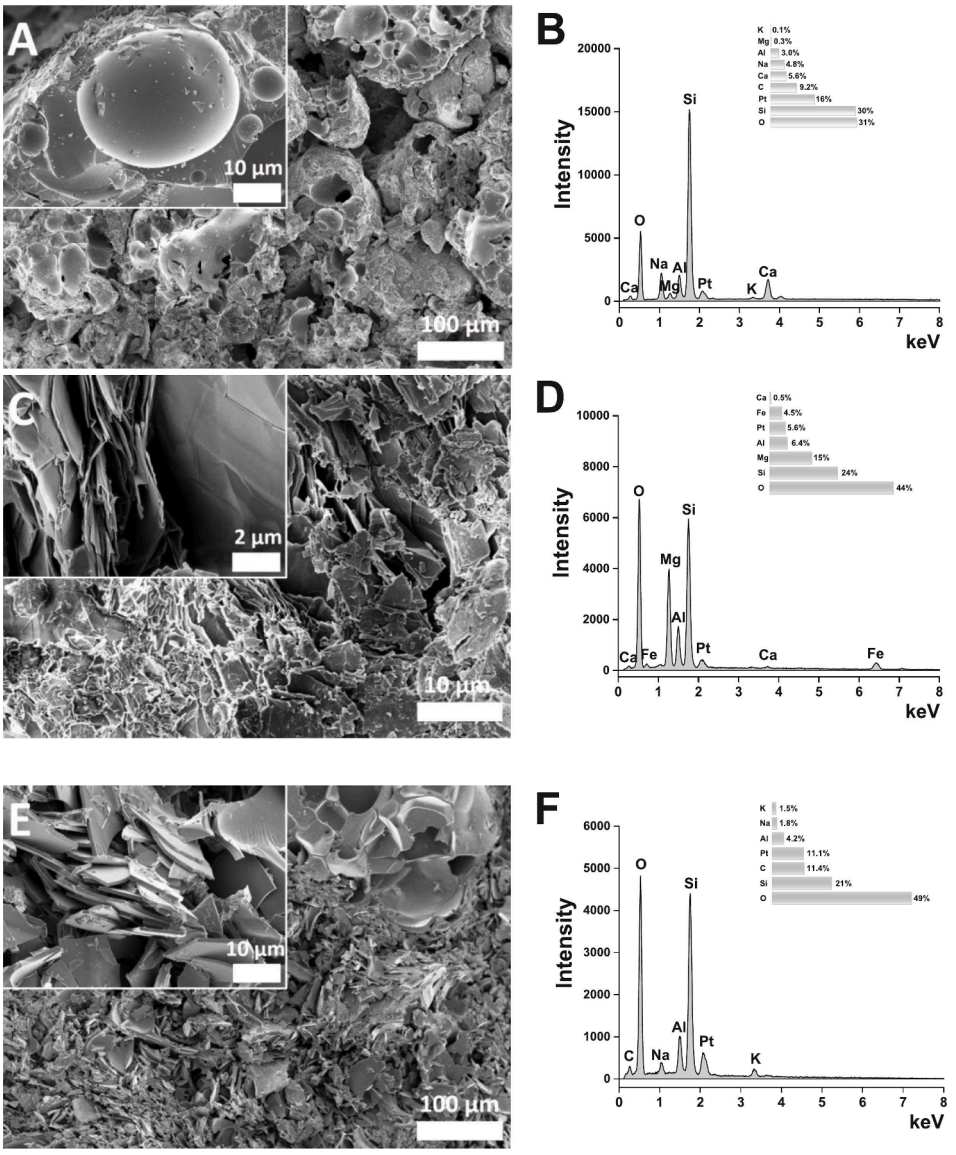


Fig 13. SEM-EDX of the inorganic based plates. (A and B) EG based plates, (C and D) EV based plate, and (E and F) EP based plate.

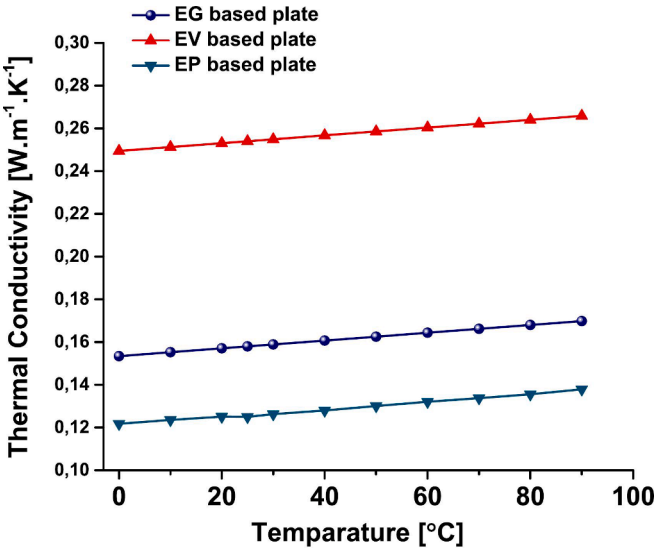


Fig. 14. Thermal conductivity of inorganic based plates.

based plate. These alterations in contact angle results for each plate are most probably due to the surface roughnesses which were measured as Ra values of 4.9 ± 0.7 µm, 9.60 ± 0.8 µm and 13.0 ± 2.5 µm for EV, EG and EP based plates, subsequently. Furthermore, this situation has also been visually analyzed with SEM micrographs where smoother surfaces have been observed for EV based plates whereas rougher surfaces have been detected for EG and EP plates. These observations have also been confirmed by previous studies in the literature [109–111].

One of the crucial problems encountered with traditional materials used in exterior facades is that the surface is not resistant to water. The penetration of rain, snow water or moisture in the air into the materials causes an increment in the thermal conductivity coefficient. Such a situation plays a kind of deteriorative role on the thermal insulation property of the materials [112,113]. Therefore, in the current study, long-term water absorption property of the inorganic based plates has been investigated and related findings are exhibited in Fig. 11C. It is clearly seen from the graph that the water absorption ratio of the EV based plate has been measured as 20.4 ± 1.8 v% in the 1st day and increased gradually to the ratio of 40.9 ± 0.3 v% in the 28th day. On the other hand, 28 days long-term immersion in water test showed that water absorption ratio of the EG based plate absorbed 10.4 ± 0.2 v% in

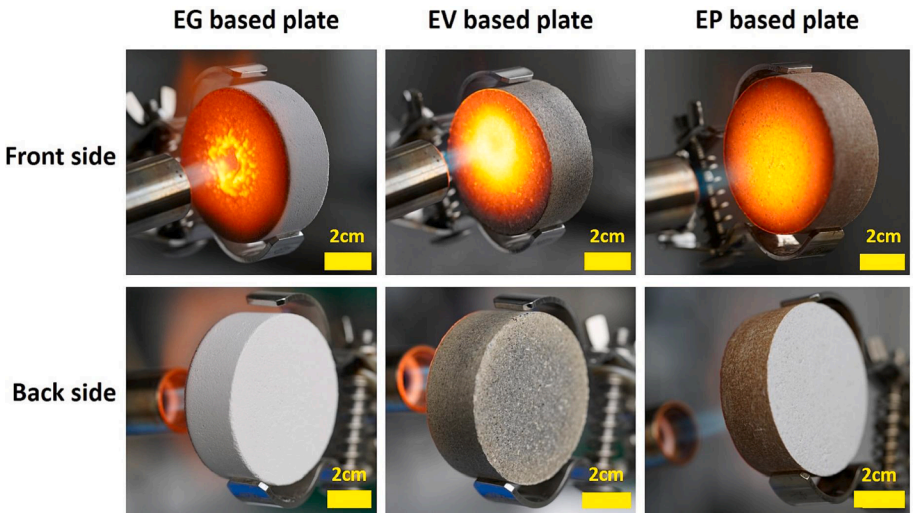


Fig. 15. The view of front and back sides of inorganic based plates after 30 min. flame exposure.

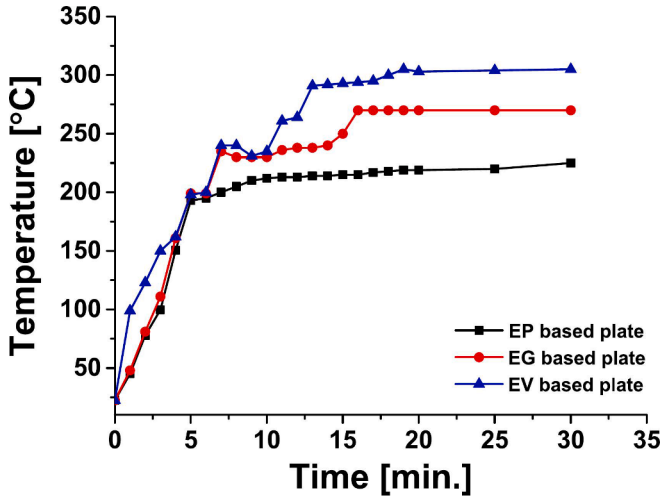


Fig. 16. The temperature change of the back sides of the inorganic based plates during 30 min. flame exposure.

the 1st day and this rate has remarkably risen to 49.8 ± 0.8 v% in the end. In the case of EP based plate, water absorption ratio has been determined as 1.76 ± 0.1 v% in the 1st day and increased slightly to 9.96 ± 0.04 v% in the 28th day. Even though it was previously reported that water absorption capacity of expanded perlite is superior due to the highly porous structure [114,115], we found that our EP based plate exhibited the lower absorption values comparing with EG and EV based plates as well as other EP based structures mentioned in the literature. For instance, Papa et. al. [116] prepared alkali bonded EP material where water stability of the samples was found as 87 ± 10 wt% at 28th day. In our study, the long-term low water absorption property of EP based plate may result from perlite's non-spherical, flake-like morphological structure.

3.5. Compressive and direct tensile strength

Mechanical properties are crucial for the practical applications of materials. In current study, mechanical performances of inorganic based plates in terms of compressive and direct tensile properties were explored. For comparison, the compressive stress-strain curves of EG and EP based plates, with a comparable density of 0.766 ± 0.009 g/cm^3 and 0.59 ± 0.006 g/cm^3, are illustrated in Fig. 12A. The compressive stress-strain curves of the samples exhibited the classic regime which comprised a linear elastic region, the plateau area and failure after densification of samples, which showed a remarkable decline in stress after a maximum load in the plateau region [117]. On the other hand, EV based plate exhibited a linear spectrum because of its ductile structure. Young's modulus of EG, EP, and EV based plates were calculated, by use of the compressive stress-strain curve slope, as 134.66 ± 1.68 MPa, 62.90 ± 1.79 MPa, and 52.40 ± 0.92 MPa, respectively. These findings also clearly proved that EV based plate was the most ductile structure, whereas EG based plate was the least one. Fig. 12B depicts the direct tensile stress-strain curves of the plates where EG based plate exhibited more brittle structure than the others, however ones again EV based plate possessed more ductile characteristics.

As a comparative representation of the materials' compressive and direct tensile properties, seen in Fig. 12C, EG based plate performed notably higher compressive and direct tensile strength values than the EP based plate, whereas the EV based plate exhibited the lowest strength among the studied plate compositions. The maximum compressive strengths of EG and EP based plates were determined as 7.04 ± 0.44 MPa and 5.82 ± 0.37 MPa, respectively. On the other hand, for EV based plate, the maximum compressive strength could not be measured since the material exhibited a ductile feature. For this reason, as mentioned in the relevant standard [53], the compressive strength at strain rate of 10 % was calculated and a value of 3.15 ± 0.17 MPa was recorded. In literature, Papa et. al. [116] studied on alkali bonded expanded perlite material and they found the compressive strength value as around 1.5 ± 0.5 MPa. In another study, Vaou and Panias [44] concentrated on preparing the perlite based geopolymers and compressive strength of the samples were reported as between 2.5 MPa and 7.8 MPa. In addition, Demirboğa and Gül [118] developed perlite based concretes and the compressive strength of the samples were recorded as 1.96 MPa. There are also some studies related to preparing expanded vermiculite and glass based materials stated in the literature. For instance, Medri et. al. [45] investigated properties of lightweight vermiculite/geopolymer based panels and they measured the compressive strength as 2 MPa. Gencel et. al. [119] conducted a research on expanded Vermiculite/fly ash based geopolymers and compressive strength values ranged between 2.8 MPa and 4.6 MPa. Shahidan et. al. [120] analyzed the compressive strength properties of expanded glass included lightweight foam concrete and the related results were 2.2 MPa. The TEOS/MTMS sol-gel bonded plates we utilized in our study provided better results than the above-mentioned literature studies. In addition, according to EN 13279 standard, compressive strength for building panels was stated as minimum 2 MPa [121]. Therefore, our results are within tolerance limits.

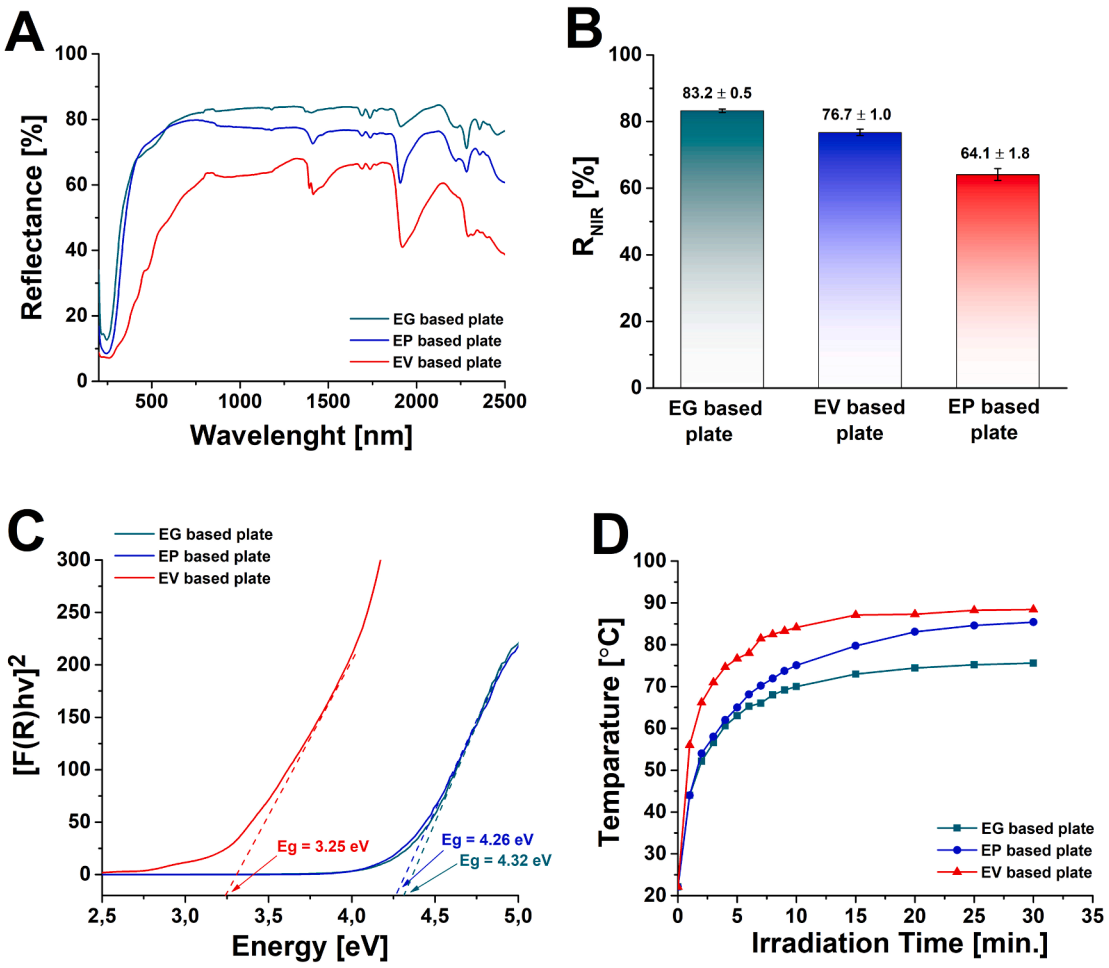


Fig. 17. NIR-reflective properties of inorganic based plates. (A) UV–vis-NIR reflectance, (B) R_{NIR} (%), (C) energy-$(F(R)hv)^2$ curves, and (D) surface temperature changes of the plates under infrared radiation over time.

Direct tensile strength analyses of inorganic based plates are important however the application of the test is not an easy task (as it has been explained in section 2.11 direct tensile strength) as a result of that this analysis have been rarely reported in literature so far. Regarding direct tensile strength results of the samples, which were in correlation with compressive strength measurements, the values were calculated as 0.486 ± 0.04 MPa, 0.417 ± 0.06 MPa, and 0.079 ± 0.04 MPa for EG, EP, and EV based plates, respectively (Fig. 12B and C).

3.6. SEM-EDX analysis

SEM micrographs in Fig. 13 (A/C/E) depicts cross sectional images of EG, EV, and EP based monolithic plates. In the images, it was observed that the EG, EV and EP particles retained their form and porous structure, however, the TEOS/MTMS sol-gel binder utilized and the compressing process generated more compact plate structures. Elemental compositions of the inorganic based plates have been illustrated in EDX graphs in Fig. 13(B/D/F). It is clearly recognized from the figures that the findings are correlated with XRF results of raw materials which are presented in Table 2. EDX graph in Fig. 13B emphasized that the distinguished sharp peak of Na was specific to EG based plate. On the other hand, another distinctive intensive peak was belonged to Mg in Fig. 13D which was obtained for EV based plate. Also, the main elements detected for all of three plates are Si, O, Al.

3.7. Thermal conductivity analysis

The effective thermal conductivity of the inorganic based plates is an important characteristic for determining their thermal properties. In Fig. 14, the thermal conductivity results of the plates are exhibited between the temperature range of 0-90ºC. It has been clearly observed that with the rising temperature, thermal conductivities of the plates were gradually increased. In literature, thermal conductivity values of EG, EP, and EV particles have been reported as 0.069–0.071 $W.m^{-1}K^{-1}$ [37], 0.063–0.068 $W.m^{-1}K^{-1}$ [3], and 0.04–0.06 $W.m^{-1}K^{-1}$ [9] at 25 °C, respectively. As can be clearly seen in the figure, after conversion of EG, EP, and EV particles to plate structures during our experiments by using synthesized TEOS/MTMS sol-gel binder, thermal conductivities of the plates were subsequently determined as 0.158 $W.m^{-1}K^{-1}$, 0.254 $W.m^{-1}K^{-1}$ and 0.125 $W.m^{-1}K^{-1}$ at 25 °C. Heat transmission occurs primarily through different ways; (1) thermal conduction through solid and gas, (2) thermal radiation between hot and cold solid surfaces, and (3) convection. In most cases, heat is transported by thermal conduction through solid. Because heat transfer by solid is easier than heat transfer via gas [122]. As a result, it is possible to explain the increment in thermal conductivity of plates comparing with the raw materials since the plate structures became more compact and solid compositions due to the existence of the TEOS/MTMS sol-gel binder. Similar results have also been reported in previous studies [34,116,123].

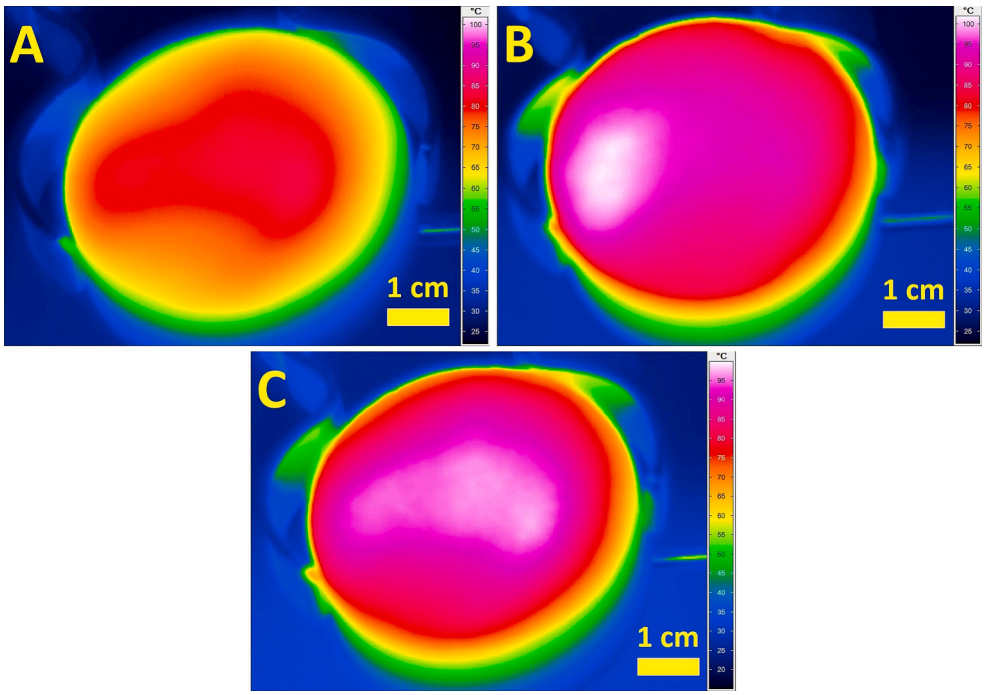


Fig. 18. Surface temperature range of the inorganic based plates under infrared radiation after 30 min. (A) EG based plate, (B) EV based plate, and (C) EP based plate.

3.8. Flame behavior of inorganic based plates

Inorganic based plates with expanded lightweight inclusions are designed as fireproof materials. As can be seen in the TGA analysis (Fig. 10B), these plates have a modest quantity of organic content which has contributed to the materials gaining fireproof properties. Fig. 15 illustrates the flame behavior of the front and back surfaces of the plates after 30 min of flame exposure. Experiments revealed that there was neither flaming combustion nor flame dissemination on the specimens, implying that the plates had outstanding flame retardant properties and could effectively prevent fire spread. On the other hand, uncombustional slight deformation has occurred on the surface of the expanded glass based plate which may be related to partial carbonization. In order to confirm the thermal resistance of the plates at high temperature (~900 °C) during the flame behavior test, back surface temperatures change of the plates were recorded by infrared thermometer (Fig. 16). As shown in the figure, temperature on the back surface of the EV based plate progressively rose up to 305 °C over the course of 19 min and remained stable until the end of test. On the other hand, the temperature on the rear surface of the EG based plate gradually increased to 270 °C within the first 16 min and remained constant till the end of the test. In the case of EP based plate, the temperature on the back surface accelerated rapidly to 195 °C in the first 5 min and continued to rise slowly to 225 °C for the next 25 min. These results are consistent with the thermal conductivity properties of the plates. Findings also revealed that inorganic based plates has great potential for developing fireproof and high temperature thermal resistant materials.

3.9. NIR-reflective properties of inorganic based plates

Due to the effects of global warming and urbanization, temperatures in urban areas are rising [124,125]. This enhances the demand for cooling electricity, increases the amount of pollutants emitted by power plants, and worsens indoor and outdoor thermal comfort [126,127]. Modification of building surfaces by using novel materials could be a countermeasure technique to tackle with negative impact of global warming and urban heat on the increment of building temperature. Solar energy consists of approximately 5 % UV, 42 % visible and 53 % near infrared radiation [128–130]. Surfaces exposed to sunlight absorb the NIR radiations which cause temperature rise, resulting in overheating of interiors and hence increased costs for air conditioning. Therefore, the NIR reflectivity of the plates used in buildings can have a significant impact on building energy efficiency. In current study, NIR reflectivity properties of the plates were investigated. The UV–visible diffuse reflectance spectra of plates from 200 to 2500 nm are illustrated in Fig. 17A. When EG, EP, and EV based plates were compared, EG based plate reflected NIR light (700–2500 nm) to the highest degree. EV based plate, on the other hand, exhibited the lowest reflectivity in this region. It has been reported that the NIR reflectance values of commercially available roofing products are determined as approximately 64 % [131]. According to our findings, EG, EP and EV based plates exhibited NIR reflectance values of 83.2 ± 0.5 %, 76.7 ± 1.0 % and 64.1 ± 1.8 %, respectively (Fig. 17B).

Fig. 17C shows energy-$(F(R)hv)^2$ curves of the plates. The band gap was calculated by plotting the quantity $(F(R)hv)^2$ against the radiation energy and is equal to the intercept of the extrapolated linear portion of the plot with the energy axis. The band gaps of the EG and EP based plates were found to be higher than the EV based plate when the graph was examined. High NIR reflectance associated with high band gap properties of the plates. When increase the band gap causes the reflect more NIR radiation and that is the reason for the increase of the NIR reflectance of plate [132]. Similar relation between band gap and NIR reflectance was mentioned in other studies in the literature as well [133,134].

The heat reflecting property of the prepared plates was also assessed by evaluating the surface temperatures for 30 min under infrared lamp radiation. Fig. 17D indicates the changes in surface temperature of the plates over time. When the surface temperatures of the EV, EP, and EG based plates were examined, they gradually elevated and then stayed steady at 88 °C, 85 °C, and 75 °C, respectively. When the plates were compared, the EG based plate had a lower surface temperature. These findings are compatible with the NIR reflectance features of the plates (Fig. 17B), where the EG based plate possessed the greatest NIR reflectance. In addition, the surface temperature range of plates under

infrared radiation after 30 min for EG, EV, and EP based plates illustrated in Fig. 18A–C, respectively.

4. Conclusion

A novel method regarding combining lightweight expanded particles, such as; glass, vermiculite and perlite, and TEOS/MTMS sol-gel binder for producing fire resistant and energy saving insulating plates has been proposed. In this study, TEOS/MTMS sol-gel binder has been successfully synthesized which performed only the weight loss of 11.4 % between 200 and 1000 °C. Also, after the plate production, it has been revealed that the binder used in the system did not change the original crystalline and amorphous structures of raw materials.

Among the all prepared inorganic based plates, EP based ones generally exhibited more sufficient physical and thermal properties. The developed EP based plate had a low density of about 0.590 ± 0.01 g/cm^3, with a thermal conductivity of 0.125 W.m^{-1}K^{-1} at 25 °C. Moreover, the plate's compressive and direct tensile strengths were 5.82 ± 0.37 MPa and 0.417 ± 0.06 MPa, respectively. Also, they had low water absorbency level of 1.76 ± 0.1 v% and 9.96 ± 0.04 v% for 1st and 28th day, subsequently. On the other hand EG based plate showed better mechanical (σ_C: 7.04 ± 0.44 MPa and σ_T: 0.486 ± 0.04 MPa) and NIR reflectance (83.2 ± 0.5 %) features.

In conclusion, our research revealed that combining various expanded lightweight particles with a TEOS/MTMS sol-gel binder could be a promising way to create a fire resistant and energy-saving insulating plates for building applications.

CRediT authorship contribution statement

Emre Yavuz: Investigation, Methodology, Writing – original draft, Writing – review & editing. **Niyazi Ugur Kockal:** Resources, Writing – review & editing. **Ramazan Erdem:** Writing – review & editing.

Declaration of Competing Interest

The authors declare the following financial interests/personal relationships which may be considered as potential competing interests: Emre Yavuz reports financial support was provided by Scientific and Technological Research Council of Turkey. Emre Yavuz reports a relationship with Council of Higher Education of the Republic of Turkey that includes: funding grants.

Data availability

No data was used for the research described in the article.

Acknowledgements

This project has received funding from the Scientific Research Projects Coordination Unit of Akdeniz University with the project code: FDK-2020-5230. The authors further acknowledge financial support by The Scientific and Technological Research Council of Türkiye (TÜBİTAK), within the programmes of 2211-C and 2214-A, and the Council of Higher Education of Türkiye by 100/2000 YÖK programme. The authors would also like to thank to Physics at Interfaces Department of Max Planck Institute for Polymer Research for their valuable support during the experimental stages of this study. The authors also wish to acknowledge Lukas Hauer for his support in calculating R_{NIR} values and video editing.

Appendix A. Supplementary data

Supplementary data to this article can be found online at https://doi.org/10.1016/j.conbuildmat.2023.130355.

References

[1] Intergovernmental Panel on Climate Change (IPCC). Climate change 2014: synthesis report. Contribution of working groups I, II and III to the Fifth assessment report of the intergovernmental Panel on climate change. 2014. p. 151. Geneva, Switzerland, https://www.ipcc.ch/site/assets/uploads/2018/05/SYR_AR5_FINAL_full_wcover.pdf.
[2] U.S. Energy Information Administration (EIA). "Energy Use in Homes". https://www.eia.gov/energyexplained/index.php?page=us_energy_homes, Son erişim tarihi:15 Haziran 2019.
[3] S. Schiavoni, F. D'Alessandro, F. Bianchi, F. Asdrubali, Insulation materials for the building sector: A review and comparative analysis, Renewable and Sustainable Energy Reviews 62 (2016) 988–1011.
[4] Baseline Energy Consumption and Greenhouse Gas Emissions in Commercial Buildings in Australia – Part 1 - Report, https://www.energy.gov.au/sites/default/files/baseline-energy-consumption-part_1-report-2012.pdf.
[5] U. Berardi, P. Jafarpur, Assessing the impact of climate change on building heating and cooling energy demand in Canada, Renewable and Sustainable Energy Reviews 121 (2020), 109681, https://doi.org/10.1016/j.rser.2019.109681.
[6] R. Ricciu, L.A. Besalduch, A. Galatioto, G. Ciulla, Thermal characterization of insulating materials, Renewable and Sustainable Energy Reviews 82 (2018) 1765–1773, https://doi.org/10.1016/j.rser.2017.06.057.
[7] A.M. Papadopoulos, State of the art in thermal insulation materials and aims for future developments, Energy and Buildings 37 (1) (2005) 77–86, https://doi.org/10.1016/j.enbuild.2004.05.006.
[8] A.A. Stec, T.R. Hull, Assessment of the fire toxicity of building insulation materials, Energy and Buildings 43 (2–3) (2011) 498–506, https://doi.org/10.1016/j.enbuild.2010.10.015.
[9] L. Aditya, T.M.I. Mahlia, B. Rismanchi, H.M. Ng, M.H. Hasan, H.S.C. Metselaar, O. Muraza, H.B. Aditiya, A review on insulation materials for energy conservation in buildings, Renewable and Sustainable Energy Reviews 73 (2017) 1352–1365, https://doi.org/10.1016/j.rser.2017.02.034.
[10] L. Wang, Z. Li, Q. Jing, P. Liu, Synthesis of composite insulation materials–expanded perlite filled with silica aerogel, Journal of Porous Materials 4 (2017) 1–10, https://doi.org/10.1007/s10934-017-0448-4.
[11] K. Sodeyama, Y. Sakka, Y. Kamino, H. Seki, Preparation of fine expanded perlite, Journal of Materials Science 34 (10) (1999) 2461–2468, https://doi.org/10.1023/A:1004579120164.
[12] O. Folorunso, C. Dodds, G. Dimitrakis, S. Kingman, Continuous energy efficient exfoliation of vermiculite through microwave heating, International Journal of Mineral Processing 114–117 (2012) 69–79, https://doi.org/10.1016/j.minpro.2012.10.003.
[13] P.M. Angelopoulos, C. Maliachova, K. Papakonstantinou, M. Taxiarchou, S. Diplas, Structural and physical characteristics of fine perlite expanded with a novel method in a vertical electric furnace, Mineral Processing and Extractive Metallurgy 125 (2) (2016) 71–80, https://doi.org/10.1080/03719553.2016.1156244.
[14] N.V. Gurgenyan, I.B. Khachanova, M.F. Kostandyan, A.E. Grigoryan, N. K. Vardanyan, Application of Qualitatively Improved Expanded Perlite (Review), Glass and Ceramics 78 (3) (2021) 161–167, https://doi.org/10.1007/s10717-021-00369-x.
[15] A.M. Rashad, A synopsis about perlite as building material – A best practice guide for Civil Engineer, Construction and Building Materials 121 (2016) 338–353, https://doi.org/10.1016/j.conbuildmat.2016.06.001.
[16] S.K. Haldar, J. Tišljar, Basic Mineralogy, Introduction to, Mineralogy and Petrology (2014) 39–79.
[17] M.S. Cetin, O. Toprakci, O.S. Taskin, A. Aksu, H.A.K. Toprakci, Expanded vermiculite-filled flexible polymer composites, Journal of Elastomers & Plastics 54 (1) (2021) 145–168, https://doi.org/10.1177/00952443211029038.
[18] M. Li, Y. Zhao, Z. Ai, H. Bai, T. Zhang, S. Song, Preparation and application of expanded and exfoliated vermiculite: A critical review, Chemical Physics 550 (2021), 111313, https://doi.org/10.1016/j.chemphys.2021.111313.
[19] A.M. Rashad, Vermiculite as a construction material – A short guide for Civil Engineer, Construction and Building Materials 125 (2016) 53–62, https://doi.org/10.1016/j.conbuildmat.2016.08.019.
[20] V.T. Shmuradko, F.I. Panteleenko, O.P. Reut, E.F. Panteleenko, N.V. Kirshina, Composition, structure, and property formation of heat insulation fire- and heat-reflecting materials based on vermiculite for industrial power generation, Refractories and Industrial Ceramics 53 (4) (2012) 254–258, https://doi.org/10.1007/s11148-012-9503-5.
[21] V.V. Budov, Hollow glass microspheres. use, properties, and technology (Review), Glass and Ceramics 51 (7) (1994) 230–235, https://doi.org/10.1007/BF00680655.
[22] L.C. Herrera-Ramírez, M. Cano, R. Guzman de Villoria, Low thermal and high electrical conductivity in hollow glass microspheres covered with carbon nanofiber–polymer composites, Composites Science and Technology 151 (2017) 211–218, https://doi.org/10.1016/j.compscitech.2017.08.020.
[23] C. Jiao, H. Wang, S. Li, X. Chen, Fire hazard reduction of hollow glass microspheres in thermoplastic polyurethane composites, Journal of hazardous materials 332 (2017) 176–184, https://doi.org/10.1016/j.jhazmat.2017.02.019.
[24] J. Sun, F. Cai, D. Tao, Q. Ni, Y. Fu, Enhanced Thermal Insulation of the Hollow Glass Microsphere/Glass Fiber Fabric Textile Composite Material, Polymers 13 (4) (2021), https://doi.org/10.3390/polym13040505.
[25] J.-P. Won, H.-B. Kang, S.-J. Lee, S.-W. Lee, J.-W. Kang, Thermal characteristics of high-strength polymer–cement composites with lightweight aggregates and

polypropylene fiber, Construction and Building Materials 25 (10) (2011) 3810–3819, https://doi.org/10.1016/j.conbuildmat.2011.03.023.
[26] J. Xiao, Y. Chen, New micro-structure designs of a polypropylene (PP) composite with improved impact property, Materials Letters 152 (2015) 210–212, https://doi.org/10.1016/j.matlet.2015.03.101.
[27] A. Das, B.K. Satapathy, Structural, thermal, mechanical and dynamic mechanical properties of cenosphere filled polypropylene composites, Materials & Design 32 (3) (2011) 1477–1484, https://doi.org/10.1016/j.matdes.2010.08.041.
[28] K.C. Yung, B.L. Zhu, T.M. Yue, C.S. Xie, Preparation and properties of hollow glass microsphere-filled epoxy-matrix composites, Composites Science and Technology 69 (2) (2009) 260–264, https://doi.org/10.1016/j.compscitech.2008.10.014.
[29] A. Krzyzak, W. Kucharczyk, J. Gaska, R. Szczepaniak, Ablative test of composites with epoxy resin and expanded perlite, Composite Structures 202 (2018) 978–987, https://doi.org/10.1016/j.compstruct.2018.05.018.
[30] A. Sethurajaperumal, A. Manohar, A. Banerjee, E. Varrla, H. Wang, K. Ostrikov, A thermally insulating vermiculite nanosheet–epoxy nanocomposite paint as a fire-resistant wood coating, Nanoscale Advances 3 (14) (2021) 4235–4243, https://doi.org/10.1039/D1NA00207D.
[31] L.G. Rabello, R. Carlos da Conceição Ribeiro, A novel vermiculite/vegetable polyurethane resin-composite for thermal insulation eco-brick production, Composites Part B, Engineering 221 (2021), 109035, https://doi.org/10.1016/j.compositesb.2021.109035.
[32] M.X. Ai, L.Q. Cao, X.L. Zhao, Z.Y. Xiang, X.Y. Guo, Preparation and Characterization of Polyurethane Rigid Foam/Expanded Perlite Thermal Insulation Composites, Advanced Materials Research 96 (2010) 141–144, https://doi.org/10.4028/www.scientific.net/AMR.96.141.
[33] Y. Chongqing, L. Shunping, Y. Jianying, N. Yong, F. Congcong, W. Hua, C. Yufeng, Preparation and Thermal Properties of Phenolic Resin/Organic Expanded Vermiculite Nanocomposites, Advanced Chemistry Letters 1 (1) (2013) 51–55, https://doi.org/10.1166/acl.2013.1004.
[34] H. Yang, Y. Jiang, H. Liu, D. Xie, C. Wan, H. Pan, S. Jiang, Mechanical, thermal and fire performance of an inorganic-organic insulation material composed of hollow glass microspheres and phenolic resin, Journal of colloid and interface science 530 (2018) 163–170, https://doi.org/10.1016/j.jcis.2018.06.075.
[35] Q.L. Yu, P. Spiesz, H.J.H. Brouwers, Development of cement-based lightweight composites – Part 1: Mix design methodology and hardened properties, Cement and Concrete Composites 44 (2013) 17–29, https://doi.org/10.1016/j.cemconcomp.2013.03.030.
[36] N.U. Kockal, F. Turker, Effect of environmental conditions on the properties of concretes with different cement types, Construction and Building Materials 21 (3) (2007) 634–645, https://doi.org/10.1016/j.conbuildmat.2005.12.004.
[37] G. Bumanis, D. Bajare, A. Korjakins, Mechanical and Thermal Properties of Lightweight Concrete Made from Expanded Glass, Journal of Sustainable Architecture and Civil, Engineering 2 (3) (2013), https://doi.org/10.5755/j01.sace.2.3.2790.
[38] F. Koksal, O. Gencel, M. Kaya, Combined effect of silica fume and expanded vermiculite on properties of lightweight mortars at ambient and elevated temperatures, Construction and Building Materials 88 (2015) 175–187, https://doi.org/10.1016/j.conbuildmat.2015.04.021.
[39] Y.H.M. Amran, R. Alyousef, H. Alabduljabbar, M. El-Zeadani, Clean production and properties of geopolymer concrete, A review, Journal of Cleaner Production 251 (2020), 119679, https://doi.org/10.1016/j.jclepro.2019.119679.
[40] E. Yavuz, N.I. Kul Gul, N.U. Kockal, Characterization of class C and F fly ashes based geopolymers incorporating silica fume, Ceramics International 48 (21) (2022) 32213–32225.
[41] J. Davidovits, Geopolymer Chemistry & Aplications, 4th Edition,, Geopolymer Institute, 2015.
[42] M.S. Tale Masoule, N. Bahrami, M. Karimzadeh, B. Mohasanati, P. Shoaei, F. Ameri, T. Ozbakkaloglu, Lightweight geopolymer concrete: A critical review on the feasibility, mixture design, durability properties, and microstructure, Ceramics International 48 (8) (2022) 10347–10371, https://doi.org/10.1016/j.ceramint.2022.01.298.
[43] N.U. Kockal, O. Beycan, N. Gulmez, Effect of binder type and content on physical and mechanical properties of geopolymers, Sādhanā 43 (4) (2018) 49, https://doi.org/10.1007/s12046-018-0806-1.
[44] V. Vaou, D. Panias, Thermal insulating foamy geopolymers from perlite, Minerals Engineering 23 (14) (2010) 1146–1151, https://doi.org/10.1016/j.mineng.2010.07.015.
[45] V. Medri, E. Papa, M. Mazzocchi, L. Laghi, M. Morganti, J. Francisconi, E. Landi, Production and characterization of lightweight vermiculite/geopolymer-based panels, Materials & Design 85 (2015) 266–274, https://doi.org/10.1016/j.matdes.2015.06.145.
[46] V.S. Le, V.V. Nguyen, A. Sharko, R. Ercoli, T.X. Nguyen, D.H. Tran, P. Łoś, K. E. Buczkowska, S. Mitura, T. Špirek, P. Louda, Fire Resistance of Geopolymer Foams Layered on Polystyrene Boards, Polymers 14 (10) (2022), https://doi.org/10.3390/polym14101945.
[47] M. Łach, Geopolymer Foams—Will They Ever Become a Viable Alternative to Popular Insulation Materials?—A Critical Opinion, Materials 14 (13) (2021) 3568.
[48] E. Nilsen, J. Puputti, M. Lindén, J. le Bell, M. Perander, M.-A. Einarsrud, Sol-Gel Derived Binder for Inorganic Composites, Journal of Sol-Gel Science and Technology 26 (1) (2003) 1239–1242, https://doi.org/10.1023/A:1020780823598.
[49] C.J. Brinker, G.W. Scherer, Sol-Gel Science: The Physics and Chemistry of Sol-Gel Processing, Academic Press, New York, 1990.
[50] H. Schmidt, G. Jonschker, S. Goedicke, M. Mennig, The Sol-Gel Process as a Basic Technology for Nanoparticle-Dispersed Inorganic-Organic Composites, Journal of Sol-Gel Science and Technology 19 (1) (2000) 39–51, https://doi.org/10.1023/A:1008706003996.
[51] Q. Wang, J. Chen, B. Gui, T. Zhai, D.a. Yang,, Fabrication and properties of thermal insulating material using hollow glass microspheres bonded by aluminum–chrome–phosphate and tetraethyl orthosilicate, Ceramics International 42 (4) (2016) 4886–4892, https://doi.org/10.1016/j.ceramint.2015.12.003.
[52] BS EN 826:2013, Thermal Insulating Products for Building Applications. Determination of Compression Behaviour, British Standards Institution 2021, www.bsigroup.com.
[53] BS EN 1607:2013, Thermal Insulating Products for Building Applications-Determination of Tensile Strength Perpendicular to Faces, British Standards Institution 2021, www.bsigroup.com.
[54] BS EN 1602:2013, Thermal Insulating Products for Building Applications. Determination of the Apparent Density, British Standards Institution 2021, www.bsigroup.com.
[55] BS EN 12087, Thermal Insulating Products for Building Applications. Determination of Long Term Water Absorption by Immersion, British Standards Institution 2021, www.bsigroup.com.
[56] BS EN 12664:2001, Thermal Performance of Building Materials and Products. Determination of Thermal Resistance by Means of Guarded Hot Plate and Heat Flow Meter Methods. Dry and Moist Products of Medium and Low Thermal Resistance, British Standards Institution 2021, www.bsigroup.com.
[57] DIN 4102-1, Fire behaviour of building materials and building components-Part 1: Building materials; concepts, requirements and tests, Deutsches Institut für Normung (DIN) 2022, www.din.de/de.
[58] ASTM E903, Standard Test Method for Solar Absorptance, Reflectance, and Transmittance of Materials Using Integrating Spheres, West Conshohocken, PA, 2020, www.astm.org.
[59] Astm g173,, Standard Tables for Reference Solar Spectral Irradiances: Direct Normal and Hemispherical on 37° Tilted Surface, ASTM International, West Conshohocken, PA, 2020.
[60] R. López, R. Gómez, Band-gap energy estimation from diffuse reflectance measurements on sol–gel and commercial TiO2: a comparative study, Journal of Sol-Gel Science and Technology 61 (1) (2011) 1–7, https://doi.org/10.1007/s10971-011-2582-9.
[61] A.S. Jbara, Z. Othaman, M.A. Saeed, Structural, morphological and optical investigations of θ-Al2O3 ultrafine powder, Journal of Alloys and Compounds 718 (2017) 1–6, https://doi.org/10.1016/j.jallcom.2017.05.085.
[62] E. Kolvari, N. Koukabi, M.M. Hosseini, Perlite: A cheap natural support for immobilization of sulfonic acid as a heterogeneous solid acid catalyst for the heterocyclic multicomponent reaction, Journal of Molecular Catalysis A: Chemical 397 (2015) 68–75, https://doi.org/10.1016/j.molcata.2014.10.026.
[63] L. Jiang, J. Wang, X. Wu, G. Zhang, A Stable Fe2O3/Expanded Perlite Composite Catalyst for Degradation of Rhodamine B in Heterogeneous Photo-Fenton System, Water, Air, & Soil Pollution 228 (12) (2017), https://doi.org/10.1007/s11270-017-3646-4.
[64] S.K. Adhikary, Z. Rudzionis, S. Tuckute, D.K. Ashish, Effects of carbon nanotubes on expanded glass and silica aerogel based lightweight concrete, Scientific reports 11 (1) (2021) 2104, https://doi.org/10.1038/s41598-021-81665-y.
[65] N.P. Shabel'skaya, E.A. Yatsenko, R.P. Medvedev, B.M. Gol'tsman, E.V. Vasil'eva, A.N. Yatsenko, Y.A. Gaidukova, Application of Foam Glass Based on Glass Scrap and Plant Ash and Slag for the Preparation of Catalytically Active Materials, Inorganic Materials 56 (7) (2020) 765–769.
[66] P.J. Launer, B. Arkles, Infrared Analysıs of Organosılıcon Compounds: Spectra-Structure Correlatıons, Silanes & Silicones, Silicon Compounds, 2003, pp. 175–178.
[67] F. Rubio, J. Rubio, J.L. Oteo, A FT-IR Study of the Hydrolysis of Tetraethylorthosilicate (TEOS), Spectroscopy Letters 31 (1) (1998) 199–219, https://doi.org/10.1080/00387019808006772.
[68] M. Montejo, F. Partal Ureña, F. Márquez, I.S. Ignatyev, J.J.L. González, Vibrational spectrum of methoxytrimethylsilane, Journal of Molecular Structure 744–747 (2005) 331–338, https://doi.org/10.1016/j.molstruc.2004.12.040.
[69] A. Venkateswara Rao, M.M. Kulkarni, D.P. Amalnerkar, T. Seth, Superhydrophobic silica aerogels based on methyltrimethoxysilane precursor, Journal of Non-Crystalline Solids 330 (1–3) (2003) 187–195, https://doi.org/10.1016/j.jnoncrysol.2003.08.048.
[70] K. Vidal, E. Gómez, A.M. Goitandia, A. Angulo-Ibáñez, E. Aranzabe, The Synthesis of a Superhydrophobic and Thermal Stable Silica Coating via Sol-Gel Process, Coatings 9 (10) (2019), https://doi.org/10.3390/coatings9100627.
[71] A.E. Charola, G.E. Wheeler, G.G. Freund, The influence of relative humidity in the polymerization of methyl trimethoxy silane, Adhesives and consolidants: Contributions to the,, IIC Congress, Paris 1984 (1984) 177–181.
[72] A.M. Barberena-Fernández, P.M. Carmona-Quiroga, M.T. Blanco-Varela, Interaction of TEOS with cementitious materials: Chemical and physical effects, Cement and Concrete Composites 55 (2015) 145–152, https://doi.org/10.1016/j.cemconcomp.2014.09.010.
[73] A. Bergantini, S. Pilling, H. Rothard, P. Boduch, D.P.P. Andrade, Processing of formic acid-containing ice by heavy and energetic cosmic ray analogues, Monthly Notices of the Royal Astronomical Society 437 (3) (2014) 2720–2727, https://doi.org/10.1093/mnras/stt2082.
[74] R. Jahanshahi, B. Akhlaghinia, Expanded perlite: an inexpensive natural efficient heterogeneous catalyst for the green and highly accelerated solvent-free synthesis

of 5-substituted-1H-tetrazoles using [bmim]N3 and nitriles, RSC Advances 5 (126) (2015) 104087–104094, https://doi.org/10.1039/C5RA21481E.
[75] T. Wei, B. Zheng, J. Liu, Y. Gao, W. Guo, Structures and thermal properties of fatty acid/expanded perlite composites as form-stable phase change materials, Energy and Buildings 68 (2014) 587–592, https://doi.org/10.1016/j.enbuild.2013.09.050.
[76] M. Dussauze, V. Rodriguez, A. Lipovski, M. Petrov, C. Smith, K. Richardson, T. Cardinal, E. Fargin, E.I. Kamitsos, How Does Thermal Poling Affect the Structure of Soda-Lime Glass? J. Phys. Chem 114 (2010) 12754–12759.
[77] A. Rincón, D. Desideri, E. Bernardo, Functional glass-ceramic foams from 'inorganic gel casting' and sintering of glass/slag mixtures, Journal of Cleaner Production 187 (2018) 250–256, https://doi.org/10.1016/j.jclepro.2018.03.065.
[78] Y. Attila, M. Güden, A. Taşdemirci, Foam glass processing using a polishing glass powder residue, Ceramics International 39 (5) (2013) 5869–5877, https://doi.org/10.1016/j.ceramint.2012.12.104.
[79] H.F. Muiambo, W.W. Focke, M. Atanasova, I.V. der Westhuizen, L.R. Tiedt, Thermal properties of sodium-exchanged palabora vermiculite, Applied Clay Science 50 (1) (2010) 51–57.
[80] H.F. Muiambo, W.W. Focke, Ion Exchanged Vermiculites with Lower Expansion Onset Temperatures, Molecular Crystals and Liquid Crystals 555 (1) (2012) 65–75, https://doi.org/10.1080/15421406.2012.634367.
[81] M.G. da Fonseca, R.K.S. Almeida, L.N.H. Arakaki, J.G.P. Espinola, C. Airoldi, Vermiculite as a useful host for guest cyclic aliphatic amine intercalation, followed by cation adsorption, Colloids and Surfaces A: Physicochemical and Engineering Aspects 280 (1) (2006) 39–44, https://doi.org/10.1016/j.colsurfa.2006.01.020.
[82] L. Chmielarz, M. Rutkowska, M. Jabłońska, A. Węgrzyn, A. Kowalczyk, P. Boroń, Z. Piwowarska, A. Matusiewicz, Acid-treated vermiculites as effective catalysts of high-temperature N2O decomposition, Applied Clay Science 101 (2014) 237–245, https://doi.org/10.1016/j.clay.2014.08.006.
[83] T. Hongo, S. Yoshino, A. Yamazaki, A. Yamasaki, S. Satokawa, Mechanochemical treatment of vermiculite in vibration milling and its effect on lead (II) adsorption ability, Applied Clay Science 70 (2012) 74–78, https://doi.org/10.1016/j.clay.2012.09.016.
[84] M. Valášková, M. Hundáková, K.M. Kutláková, J. Seidlerová, P. Čapková, E. Pazdziora, K. Matějová, M. Heřmánek, V. Klemm, D. Rafaja, Preparation and characterization of antibacterial silver/vermiculites and silver/montmorillonites, Geochimica et Cosmochimica Acta 74 (22) (2010) 6287–6300, https://doi.org/10.1016/j.gca.2010.08.025.
[85] L. Chmielarz, A. Kowalczyk, M. Michalik, B. Dudek, Z. Piwowarska, A. Matusiewicz, Acid-activated vermiculites and phlogophites as catalysts for the DeNOx process, Applied Clay Science 49 (3) (2010) 156–162, https://doi.org/10.1016/j.clay.2010.04.020.
[86] A. Majouli, S.A. Younssi, S. Tahiri, A. Albizane, H. Loukili, M. Belhaj, Characterization of flat membrane support elaborated from local Moroccan Perlite, Desalination 277 (1–3) (2011) 61–66, https://doi.org/10.1016/j.desal.2011.04.003.
[87] A. Majouli, S.A. Younssi, S. Tahiri, A. Albizane, H. Loukili, M. Belhaj, Characterization of flat membrane support elaborated from local Moroccan Perlite, Desalination 277 (1) (2011) 61–66, https://doi.org/10.1016/j.desal.2011.04.003.
[88] R. Al-Oweini, H. El-Rassy, Synthesis and characterization by FTIR spectroscopy of silica aerogels prepared using several Si(OR)4 and R′′Si(OR′)3 precursors, Journal of Molecular Structure 919 (1–3) (2009) 140–145, https://doi.org/10.1016/j.molstruc.2008.08.025.
[89] S.V. Ingale, P.B. Wagh, A.K. Tripathi, V.S. Kamble, R. Kumar, S.C. Gupta, Physico-chemical properties of silica aerogels prepared from TMOS/MTMS mixtures, Journal of Porous Materials 18 (5) (2010) 567–572, https://doi.org/10.1007/s10934-010-9410-4.
[90] S. Amoriello, A. Bianco, L. Eusebio, P. Gronchi, Evolution of two acid steps sol–gel phases by FTIR, Journal of Sol-Gel Science and Technology 58 (1) (2010) 209–217, https://doi.org/10.1007/s10971-010-2379-2.
[91] D. Kim, J. Matyáš, Batch Reactions of a Soda-Lime Silicate Glass, (Report for G Plus Project for Libbey Inc.), 2002.
[92] J.C. Swanepoel, C.A. Strydom, Utilisation of fly ash in a geopolymeric material, Applied Geochemistry 17 (8) (2002) 1143–1148, https://doi.org/10.1016/S0883-2927(02)00005-7.
[93] K.S. Hong, R.F. Speyer, Thermal Analysis of Reactions in Soda-Lime Silicate Glass Batches Containing Melting Accelerants: I, One- and Two-Component Systems, Journal of the American Ceramic Society 76 (3) (1993) 598–604, https://doi.org/10.1111/j.1151-2916.1993.tb03647.x.
[94] R. Anantha Narayanan, V. Subramanian, P. Sahoo, J. Misra, A. Kumar, R. Baskaran, B. Venkatraman, N. Murali, Experimental investigations on carbonation of sodium aerosol generated from sodium fire in the context of fast reactor safety, Annals of Nuclear Energy 80 (2015) 188–194, https://doi.org/10.1016/j.anucene.2014.12.033.
[95] L. Ma, X. Su, Y. Xi, J. Wei, X. Liang, J. Zhu, H. He, The structural change of vermiculite during dehydration processes: A real-time in-situ XRD method, Applied Clay Science 183 (2019), 105332, https://doi.org/10.1016/j.clay.2019.105332.
[96] A. Marzec, B. Szadkowski, J. Rogowski, P. Rybiński, W. Maniukiewicz, Novel eco-friendly hybrid pigment with improved stability as a multifunctional additive for elastomer composites with reduced flammability and pH sensing properties, Dyes and Pigments 186 (2021), 108965, https://doi.org/10.1016/j.dyepig.2020.108965.
[97] A. Arguelles, M. Leoni, J.A. Blanco, C. Marcos, Semi-ordered crystalline structure of the Santa Olalla vermiculite inferred from X-ray powder diffraction, American Mineralogist 95 (1) (2009) 126–134, https://doi.org/10.2138/am.2010.3249.
[98] M. Roulia, K. Chassapis, J.A. Kapoutsis, E.I. Kamitsos, T. Savvidis, Influence of thermal treatment on the water release and the glassy structure of perlite, Journal of Materials Science 41 (18) (2006) 5870–5881, https://doi.org/10.1007/s10853-006-0325-z.
[99] Z. Li, Y. Zhang, S. Huang, X. Wu, L. Shi, Q. Liu, Thermal stability and pyrolysis characteristics of MTMS aerogels prepared in pure water, Journal of Nanoparticle Research 22 (10) (2020), https://doi.org/10.1007/s11051-020-05062-8.
[100] V.S. Smitha, P.M.A. Azeez, K.G. Warrier, B.N. Nair, U.N.S. Hareesh, Transparent and Hydrophobic MTMS/GPTMS Hybrid Aerogel Monoliths and Coatings by Sol-Gel Method: A Viable Remedy for Oil-Spill Cleanup, ChemistrySelect 3 (11) (2018) 2989–2997, https://doi.org/10.1002/slct.201702967.
[101] S. He, Y. Huang, G. Chen, M. Feng, H. Dai, B. Yuan, X. Chen, Effect of heat treatment on hydrophobic silica aerogel, Journal of hazardous materials 362 (2019) 294–302, https://doi.org/10.1016/j.jhazmat.2018.08.087.
[102] M.A. Presley, P.R. Christensen, Thermal conductivity measurements of particulate materials: 4. Effect of bulk density for granular particles, Journal of Geophysical Research: Planets 115 (E7) (2010), https://doi.org/10.1029/2009JE003482.
[103] J. He, H. Wu, L. Zhong, Q. Zhong, Q. Yang, X. Ye, Z. Liu, Y. Kang, Mechanical properties and thermal conductivity of lightweight and high-strength carbon-graphite thermal insulation materials, Journal of Materials Science 57 (6) (2022) 4166–4179, https://doi.org/10.1007/s10853-021-06862-6.
[104] S. Rajpoot, R. Malik, Y.-W. Kim, Effects of polysiloxane on thermal conductivity and compressive strength of porous silica ceramics, Ceramics International 45 (17) (2019) 21270–21277, https://doi.org/10.1016/j.ceramint.2019.07.109.
[105] J. Khedari, B. Suttisonk, N. Pratinthong, J. Hirunlabh, New lightweight composite construction materials with low thermal conductivity, Cement and Concrete Composites 23 (1) (2001) 65–70, https://doi.org/10.1016/S0958-9465(00)00072-X.
[106] G.C. Tatlisu, C. Aciksari, S. Celebi, S. Turan, Developing a hollow glass microsphere/geopolymer thermal insulation composite for hot metal surface coating, Ceramics International 48 (9) (2022) 11924–11939, https://doi.org/10.1016/j.ceramint.2022.01.042.
[107] K. Grundke, K. Pöschel, A. Synytska, R. Frenzel, A. Drechsler, M. Nitschke, A. L. Cordeiro, P. Uhlmann, P.B. Welzel, Experimental studies of contact angle hysteresis phenomena on polymer surfaces — Toward the understanding and control of wettability for different applications, Advances in Colloid and Interface Science 222 (2015) 350–376, https://doi.org/10.1016/j.cis.2014.10.012.
[108] R. Erdem, M. Yüksek, E. Sancak, O. Atak, M. Erginer, L. Kabasakal, A. Beyit, Electrospinning of single and multilayered scaffolds for tissue engineering applications, The Journal of The Textile Institute 108 (6) (2017) 935–946, https://doi.org/10.1080/00405000.2016.1204900.
[109] M.R. Ricciardi, I. Papa, G. Coppola, V. Lopresto, L. Sansone, V. Antonucci, Effect of Plasma Treatment on the Impact Behavior of Epoxy/Basalt Fiber-Reinforced Composites: A Preliminary Study, Polymers 13 (8) (2021), https://doi.org/10.3390/polym13081293.
[110] N. Hideo, I. Ryuichi, H. Yosuke, S. Hiroyuki, Effects of surface roughness on wettability, Acta Materialia 46 (7) (1998) 2313–2318, https://doi.org/10.1016/S1359-6454(98)80012-8.
[111] D.P. Dowling, I.S. Miller, M. Ardhaoui, W.M. Gallagher, Effect of surface wettability and topography on the adhesion of osteosarcoma cells on plasma-modified polystyrene, Journal of biomaterials applications 26 (3) (2011) 327–347, https://doi.org/10.1177/0885328210372148.
[112] S. Cai, B. Zhang, L. Cremaschi, Review of moisture behavior and thermal performance of polystyrene insulation in building applications, Building and Environment 123 (2017) 50–65, https://doi.org/10.1016/j.buildenv.2017.06.034.
[113] A. Szymczak-Graczyk, G. Gajewska, I. Laks, W. Kostrzewski, Influence of Variable Moisture Conditions on the Value of the Thermal Conductivity of Selected Insulation Materials Used in Passive Buildings, Energies 15 (7) (2022) 2626, https://doi.org/10.3390/en15072626.
[114] O. Sengul, S. Azizi, F. Karaosmanoglu, M.A. Tasdemir, Effect of expanded perlite on the mechanical properties and thermal conductivity of lightweight concrete, Energy and Buildings 43 (2–3) (2011) 671–676, https://doi.org/10.1016/j.enbuild.2010.11.008.
[115] H. Xiong, K. Yuan, J. Xu, M. Wen, Pore structure, adsorption, and water absorption of expanded perlite mortar in external thermal insulation composite system during aging, Cement and Concrete Composites 116 (2021), 103900, https://doi.org/10.1016/j.cemconcomp.2020.103900.
[116] E. Papa, V. Medri, A. Natali Murri, L. Laghi, G. De Aloysio, S. Bandini, E. Landi, Characterization of alkali bonded expanded perlite, Construction and Building Materials 191 (2018) 1139–1147, https://doi.org/10.1016/j.conbuildmat.2018.10.086.
[117] X. Gao, L. Zhou, X. Ren, J. Li, Rate effect on the stress–strain behavior of concrete under uniaxial tensile stress, Structural Concrete 22 (S1) (2020), https://doi.org/10.1002/suco.201900567.
[118] R. Demirboğa, R. Gül, Thermal conductivity and compressive strength of expanded perlite aggregate concrete with mineral admixtures, Energy and Buildings 35 (11) (2003) 1155–1159, https://doi.org/10.1016/j.enbuild.2003.09.002.
[119] O. Gencel, A. Gholampour, H. Tokay, T. Ozbakkaloglu, Replacement of Natural Sand with Expanded Vermiculite in Fly Ash-Based Geopolymer Mortars, Applied Sciences 11 (4) (2021) 1917, https://doi.org/10.3390/app11041917.

[120] S. Shahidan, E. Aminuddin, K. Mohd Noor, N.I.R. Ramzi Hannan, N.A. Saiful Bahari, M.J. Zainorizuan, L. Yee Yong, L. Alvin John Meng Siang, O. Mohamad Hanifi, R. Siti Nazahiyah, A. Mohd Shalahuddin, Potential of Hollow Glass Microsphere as Cement Replacement for Lightweight Foam Concrete on Thermal Insulation Performance, MATEC Web Conf. 103 (2017) 01014.
[121] BS EN 13279, Gypsum binders and gypsum plasters Part 1: Definitions and requirements, British Standards Institution 2008, www.bsigroup.com.
[122] J.Z. Liang, F.H. Li, Simulation of heat transfer in hollow-glass-bead-filled polypropylene composites by finite element method, Polymer Testing 26 (3) (2007) 419–424, https://doi.org/10.1016/j.polymertesting.2006.12.014.
[123] J. Gao, J. Wang, H. Xu, C. Wu, Preparation and properties of hollow glass bead filled silicone rubber foams with low thermal conductivity, Materials & Design 46 (2013) 491–496, https://doi.org/10.1016/j.matdes.2012.08.070.
[124] A.J. Arnfield, Two decades of urban climate research: a review of turbulence, exchanges of energy and water, and the urban heat island, International Journal of Climatology 23 (1) (2003) 1–26, https://doi.org/10.1002/joc.859.
[125] S. Yumino, T. Uchida, K. Sasaki, H. Kobayashi, A. Mochida, Total assessment for various environmentally conscious techniques from three perspectives: Mitigation of global warming, mitigation of UHIs, and adaptation to urban warming, Sustainable Cities and Society 19 (2015) 236–249, https://doi.org/10.1016/j.scs.2015.05.010.
[126] M. Santamouris, C. Cartalis, A. Synnefa, D. Kolokotsa, On the impact of urban heat island and global warming on the power demand and electricity consumption of buildings—A review, Energy and Buildings 98 (2015) 119–124, https://doi.org/10.1016/j.enbuild.2014.09.052.
[127] C. Cartalis, A. Synodinou, M. Proedrou, A. Tsangrassoulis, M. Santamouris, Modifications in energy demand in urban areas as a result of climate changes: an assessment for the southeast Mediterranean region, Energy Conversion and Management 42 (14) (2001) 1647–1656, https://doi.org/10.1016/S0196-8904(00)00156-4.
[128] R. Levinson, P. Berdahl, H. Akbari, Solar spectral optical properties of pigments—Part I: model for deriving scattering and absorption coefficients from transmittance and reflectance measurements, Solar Energy Materials and Solar Cells 89 (4) (2005) 319–349, https://doi.org/10.1016/j.solmat.2004.11.012.
[129] B. Kaur, N. Quazi, I. Ivanov, S.N. Bhattacharya, Near-infrared reflective properties of perylene derivatives, Dyes and Pigments 92 (3) (2012) 1108–1113, https://doi.org/10.1016/j.dyepig.2011.06.011.
[130] S.P. Radhika, K.J. Sreeram, B. Unni Nair, Mo-Doped Cerium Gadolinium Oxide as Environmentally Sustainable Yellow Pigments, ACS Sustainable Chem. Eng. 2 (5) (2014) 1251–1256.
[131] K.L. Uemoto, N.M.N. Sato, V.M. John, Estimating thermal performance of cool colored paints, Energy and Buildings 42 (1) (2010) 17–22, https://doi.org/10.1016/j.enbuild.2009.07.026.
[132] A. Rosati, M. Fedel, S. Rossi, NIR reflective pigments for cool roof applications: A comprehensive review, Journal of Cleaner Production 313 (2021), 127826, https://doi.org/10.1016/j.jclepro.2021.127826.
[133] Q. Gao, X. Wu, Y. Fan, Q. Meng, Novel near infrared reflective pigments based on hollow glass microsphere/BiOCl1-xIx composites: Optical property and superhydrophobicity, Solar Energy Materials and Solar Cells 180 (2018) 138–147, https://doi.org/10.1016/j.solmat.2018.02.033.
[134] L. Liu, A. Han, M. Ye, W. Feng, The evaluation of thermal performance of cool coatings colored with high near-infrared reflective nano-brown inorganic pigments: Magnesium doped ZnFe2O4 compounds, Solar Energy 113 (2015) 48–56, https://doi.org/10.1016/j.solener.2014.12.034.